Embedded Vector Measurement of RF/Microwave Circuits in LTCC Technology

by

Hana MOHAMED

THESIS PRESENTED TO ÉCOLE DE TECHNOLOGIE SUPÉRIEURE
IN PARTIAL FULFILLMENT FOR A MASTER'S DEGREE
WITH THESIS IN ELECTRICAL ENGINEERING
M.A.Sc.

MONTREAL, MAY 8, 2019

ÉCOLE DE TECHNOLOGIE SUPÉRIEURE
UNIVERSITÉ DU QUÉBEC

 Hana Mohamed, 2019

This Creative Commons licence allows readers to download this work and share it with others as long as the author is credited. The content of this work can't be modified in any way or used commercially.

BOARD OF EXAMINERS

THIS THESIS HAS BEEN EVALUATED

BY THE FOLLOWING BOARD OF EXAMINERS

Mr. Ammar B. Kouki, Thesis Supervisor
Department of Electrical Engineering at École de technologiesupérieure

Mr. NaimBatani, President of the Board of Examiners
Department of Electrical Engineering at École de technologiesupérieure

Mr. Francois Gagnon, Member of the Board of Examiners
Department of Electrical Engineering at École de technologiesupérieure

THIS THESIS WAS PRENSENTED AND DEFENDED

IN THE PRESENCE OF A BOARD OF EXAMINERS AND PUBLIC

18 OF APRIL 2019

AT ÉCOLE DE TECHNOLOGIE SUPÉRIEURE

ACKNOWLEDGMENT

I would like to take this opportunity to thank all the students and the members of LACIME laboratory for their generous support during this research project.

First of all, I would like to express my gratitude to my ebullient supervisor, Prof. Ammar B. Kouki for his wonderful support, encouragement, and advices to complete the research project successfully. I would also like to thank Mr. Normand Gravel for his patience and assistance in fabricating the many prototypes of my designs. Further, I am also thankful to my colleagues in ÉTS for their constant support and assistance during the research work.

I also appreciate the Ministry of Education of Libya for their financial support of my own studies and that of the entire Libyan student community who are pursuing Masters and PhD studies in Canada. I am also thankful to my family in Libya: my father, mother, and brother who advised and encouraged me to pursue graduate studies in Canada. Finally, I am humbled by the patience and support provided by my husband, daughter and son during my studies. I dedicate this project to my country Libya, my family, and my friends.

I am glad to work and study in ÉTS where scientific research goes parallel with latest industrial technology. The international atmosphere at ÉTS helped me to showcase my technical expertise and enhanced my knowledge.

Mesure vectorielle intégrée de circuits RF / micro-ondes dans la technologie LTCC

Hana MOHAMED

RESUME

Alors que le nombre de systèmes et de normes sans fil continuent à augmenter, la réutilisation de matériel RF devient de plus en plus importante pour réduire les coûts et la taille et éliminer la redondance inutile des composants. Un moyen de maximiser la réutilisation du matériel RF consiste à déployer des circuits reconfigurables. Cela dépend à son tour de la mesure vectorielle intégrée pour garantir le bon fonctionnement du matériel reconfigurable.

Les techniques classiques de mesure vectorielle nécessitent des analyseurs de réseau vectoriel coûteux et encombrants ou des jonctions six ports légèrement plus compactes. Les deux options nécessitent l'utilisation de coupleurs directionnels pour l'échantillonnage des ondes progressives, ce qui augmente leur taille et limite leur aptitude à l'intégration dans du matériel RF reconfigurable. Les interféromètres à quatre ports non directionnels offrent une solution alternative pour la mesure vectorielle intégrée, caractérisée par une très petite taille, un très faible couplage et une facilité d'intégration.

Dans le présent travail, un nouveau réflectomètre 3D non directionnel à 4 ports pour la mesure de coefficients de réflexion complexes est proposé. Le réflectomètre proposé comporte deux renifleurs non directionnels optimisés placés sous une ligne de transmission avec des lignes enterrées pour acheminer les signaux reniflés aux détecteurs de puissance de la technologie LTCC. Les transitions verticales des lignes enterrées à la surface sont conçues et optimisées. Des simulations de champs électromagnétiques en 3D permettent d'optimiser la conception proposée afin d'obtenir le paramètre S de la structure. Deux circuits de détection de puissance LT5582 avec une plage dynamique de 57 dB sont utilisés pour détecter la puissance couplée. Un prototype du réflectomètre proposé est fabriqué au LTCC (Ferro L8) dans le laboratoire LACIME et utilisé pour mesurer 45 charges complexes différentes. Les résultats obtenus montrent un excellent accord avec les mesures VNA montrant des erreurs inférieures à 0,3 dB pour l'amplitude et inférieures à 3 ° pour la phase.

Mots clés: réflectomètre, coefficient de réflexion, puissance couplée, paramètres S, LTCC

Embedded Vector Measurement of RF/Microwave Circuits in LTCC Technology

Hana MOHAMED

ABSTRACT

As the number of wireless systems and standards continues to increase, RF hardware re-use is becoming more and more important to reduce cost and size and eliminate unnecessary component redundancy. One way of maximizing RF hardware re-use is to deploy reconfigurable circuits. This is turn relies on embedded vector measurement to ensure the reconfigurable hardware operates as required.

Conventional vector measurement techniques require costly and bulky Vector network analyzers or slightly more compact six-port junctions. Both options require the use directional couplers to sample forward and backward traveling waves, which increases their size and limits their suitability for embedding in reconfigurable RF hardware. Non-directional four-port interferometersoffer an alternative solution for embedded vector measurement that is characterized bya very small size, very low coupling, and ease of integration.

In the present work, a new 3D 4-port non-directional reflectometer for measuring complex reflection coefficients is proposed. The proposed reflectometer features two optimized non-directional sniffers positioned below a transmission line with buried lines to carry the sniffed signals to power detectors in LTCC technology. Vertical transitions from the buried lines to surface are designed and optimized. 3D electromagnetic field simulations are used to optimize the proposed design in order to obtain the S-parameter of the structure. Two LT5582 power detector circuits with 57 dB dynamic range are used to detect the coupled power. A prototype of the proposed reflectometer is fabricated in LTCC (Ferro L8) in LACIME laboratory and used to measure 45 different complex loads. The obtained results show excellent agreement with VNA measurements showing errors below 0.3 dB for amplitude and below 3° for phase.

Key words: Reflectometer, reflection coefficient, coupled power, S-parameters, LTCC

TABLE OF CONTENTS

Page

LIST OF TABLES

Page

LIST OF FIGURES

Page

LIST OF ABREVIATIONS

AC	Alternating current.
AD8302	Analog Device 8302.
CPW	Coplanar Waveguide.
CW	Continuous wave.
dB	Decibel.
DC	Direct Current.
DUTs	Device under tests.
EM	Electromagnetic.
IoT	Internet of things.
IL	Insertion losses.
LTCC	low temperature co-fired ceramic.
LT5582	Linear Technology 5582.
ML	Microstripline.
RF	Radio Frequency.

RL	Return Losses.
RMS	Root Mean Square.
SOLR	Short-Open-Load-Reciprocal.
SOLT	Short-Open-Load-Through.
SNAs	Scalar Network Analyzers.
TL	Transmission line.
V	Volt.
VNA	Vector Network Analyzer.
Z_L	Load Impedance.
Z0	Characteristic Impedance.
Ω	Ohm.
3D	Tree-dimensional.
Γ	Reflection Coefficient.
λ	Electrical Wavelength.

INTRODUCTION

Microwave engineering and its applications have continued to grow over the last few years fueled by growth in many wireless communication technologies such as 5G (Wi-Fi) and the Internet of Things (IoT). By connecting more and more devices (such as cellphones, home appliance, vehicles, and others) that sense and collect data from different sources and share this data over the area where the Internet is accessible, there is an increased need for better electromagnetic spectrum usage with maintained high transmission quality. Recently, multiple antennas have been used in Multiple Input Multiple Output (MIMO) systems to increase spectrum efficiency, see for example (S. Abdulrab, M. R. Islam, M, et al, 2016). Cognitive Radio techniques offer even means for even further spectrum efficiency increase (C. Park, et al., 2007) while Software Defined Radio (SDR) techniques provide techniques that also help to maximize the use of limited spectrum (R. Zitouni and L. George, 2016). In many of these techniques, reconfiguration of the radio communication system is employed to achieve the desired spectrum efficiency improvement. At the RF level, this requires very wideband systems or, preferably, reconfigurable front-ends. Figure 0.1 illustrates a RF front-ends configuration for multi-band communicating system which consists of RFIC, PAs, LNAs, filters, duplexers, and antenna switches (H. Okazaki, T. Furuta, et al, 2013).

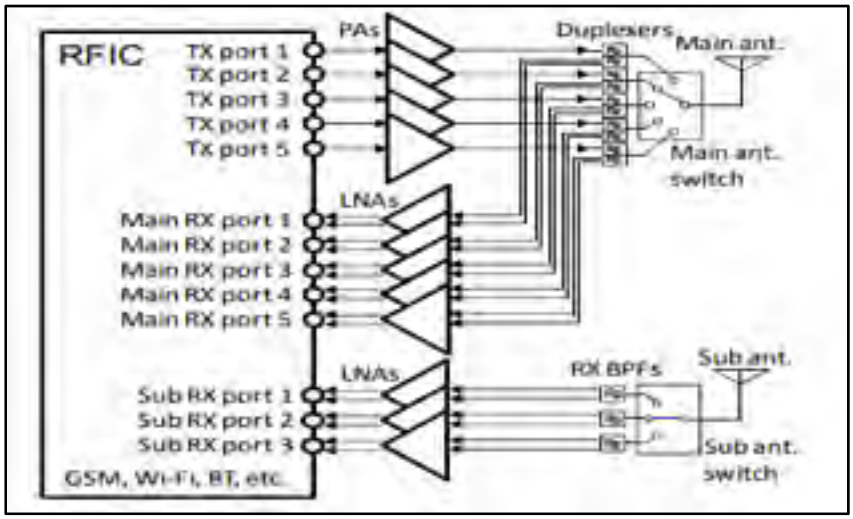

Figure 0.1 RF front-end configuration of multi-band terminal.
Taken from H. Okazaki, T. Furuta, and et al (2013, pg.432)

To adjust the front-end at the desired frequency, broadband matching and using reconfigurable or variable devices can be used. Figure 0.2 illustrates amplifier consists of a GaAs FET, two matching networks (MNs) at the input and output of the the transistor with MEMs switches(H. Okazaki, T. Furuta, et al, 2013) (F. Domingue, S. Fouladi, A. B. Kouki and R. Mansour, 2009). However, there is still a challenge of determining the precise response of a front-end, or its sub-blocs, as it is being reconfigured or tuned to a different frequencies (Ammar B. Kouki et al, 2010).

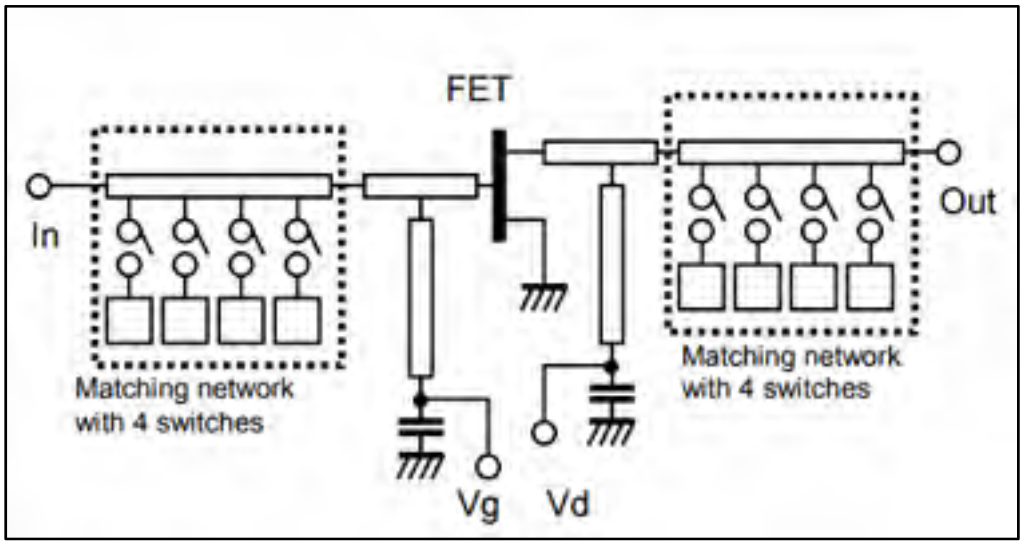

Figure 0.2 Block diagram of reconfigurable Amplifier
Taken from H. Okazaki, T. Furuta, and et al (2013, pg.432)

In this context, there is a need for embedded measurements of RF circuits and devices. In particular, embedded vector RF measurements, traditionally only accessible with commercial bulky and expensive vector network analyzers (D. Fei, 2013), are needed to enable in situ monitoring and reconfiguring of RF circuits and systems. One potential approach to achieve this is to use the 6-port technique (F. M. Ghannouchi& A. Mohammadi, 2009), which uses several individual power measurements along with a dedicated algorithm to perform vector measurements of reflection coefficients. Another alternative technique for RF vector measurements can be found in the gain and phase detection circuit made by Analog Devices, which includes demodulating logarithmic amplifiers with dynamic range of 60 dB.While either of the above-mentioned methods can be used with relative success, they have their

drawbacks. As discussed, vector network analyzers are expensive and bulky and are, therefore, not suitable for embedded measurements. The 6-port method requires two directional couplers, which are used to sample the forward and backward signal (A. Eroglu, et al,2010)and multiple power dividers and power detectors leading to a large circuit. Analog Devices' gain and phase detection circuit also needs directional coupler as well and other analog components, which can lead to a large size not suitable for embedding in RF front-end circuitry (R. Malmqvist et al., 2010).

In 2010, a new approach for embedded vector measurement was proposed based on a four-port reflectometer that uses two non-directional signal sniffers and a signal carrying transmission line (TL) all in Microstrip technology. The sniffers were made of regular microstrip lines positioned close to the signal-carrying line at a 90^{o} angle to it. One port of the signal carrying line is used to connect RF input signal while the other port is used to connect the load to be measured. At the end of each of the two sniffer lines, a power detector is connected to measure the non-directionally sampled power. These sniffers are extremely simple, have extremely small size, and provide very low coupling (-30 dB) which make the reflectometer more convenient for integration in the embedded system. Because of having a very low coupling factor, the sniffers will not have any effect on the propagation of the power signal in the system. This design provided a good agreement between the measurement using vector network analyzer and the proposed four-port reflectometer with magnitude errors less than 0.8 dB and phase errors less than 6^{o} (A. B. Kouki, et al., 2010).

Research Problem

Having the sniffers and the signal carrying transmission line on the same layer can cause undesirableinterference and will increase the layout complexity when additional signal or bias lines need to be routed on the same layer. Therefore, finding novel four-port reflectometer structures that preserve the advantages of non-directional sniffers while addressing the potential interference and layout complexity problems constitutes the research

problem to be addressed in this project. LTCC technology will be used for the development and implementation of possible solutions to the stated problem.

Research Objective

The main objective of this work is to investigate and design four-port reflectometers in 3D multilayer structures using vertical non-directional sniffers (partially filled vias) that can be placed underneath the signal carrying transmission line instead of being on the same layer. The strategy of using vertical non-directional sniffers to design the reflectometer can provide very low coupling (below -30 dB), reduce the cost, not interfere with the signal/bias carrying lines, and lead to very small size. All of these features make the sought 3D four-port reflectometer appropriate for circuit integration and embedded vector measurement. LTCC technology is the suitable 3D multilayer fabrication technology that will be used for the design and fabrication of the proposed reflectometer. The targeted measurement precision is expected to be similar to commercial VNAs but without necessarily having comparable dynamic range as the reflectometer is not expected to serve as a measurement instrument.

Contributions

The results of the present project were the subject of a conference paper entitled: "3D Reflectometer Design for Embedded RF Vector Measurement" that has been accepted for publication at the 92nd ARFTG Microwave Measurement Symposium in Orlando, Florida. ARFTG is the main microwave measurement conference (see APENDEX I).

Thesis Organization

In this thesis, chapter 1 presents different alternative techniques that provide RF vector measurements starting from vector network and its types: scalar network analyzer and vector network analyzer to the six-port technique to gain and phase detection using Analog Devices' AD3202. Chapter 2 covers the alternative non-directional reflectometer technique with the ability of integration for embedded vector measurement. Both the planar version, using a

microstrip line and two very simple sniffers as well as will present the new 3D structure are presented. The theory for computing the reflection coefficient of a given load, or device under test (DUT) is also developed in this chapter. Chapter 3 presents the methodology for designing and simulating the 3D reflectometer using 3D electromagnetic field simulation. Fabrication of the proposed 3D reflectometer using LTCC technology is also discussed. Measurement of several loads using the fabricated reflectometer and a commercial VNA and presented and compared. Finally, a conclusion and recommendations for future works complete the thesis.

CHAPTER 1

VECTOR MEASUREMENT TECHNIQUES

1.1 Introduction

Microwave technology has experienced unprecedented growth over the past few decades. However, this growth spurt is also bringing with it some challenges with regard to the need for increasingly precise vector and scalar measurements. Scalar measurement is acquired viaamplitude only measurement while vector measurements are madeon signal phases as well as amplitutudes. For standing wave ratios, signal loss or power measurements, scalar measurements usually suffice, whereas for measuring antenna phasing, in-depth circuit descriptions and impedances, vector measurements instead of scalar are optimal. It is worth noting that vector measurements play a critical role in other fields besides microwave technolgy. For instance, they are key elements in diagnostics, medicine (W. C.Khor and M. E. Bialkowski, 2006) (W. C. Khor, M. E. Biakowski, et al, 2007, and a wide range of industrial applications (G. Vinci and A. Koelpin, 2016)(B. Sopori, et al, 2000).

Vector measurements are typically made by employing a vector network analyzer. This tool enables precise measurements to be made across a broad frequency band, measuring for signal phases in addition to amplitude. However, vector network analyzers are currently quite costly due to their complex design. Therefore, researchers are looking to other strategies and approaches to obtain the required vector measurements. One of the more popular methods used in various fields today is the sixport method, which employs four separate power measurements as a means to find the reflection coefficient. Further, vector measurement can be accomplished by dedicated circuitry such as the commercial gain and phase detection circuits. In the following, embedded vector measurement through 3D reflectometers is presented as an alternative new technique that can address some of the limitations of the existing ones.

1.2 Architectures of Network Analyzers

Scalar network analyzers have traditionally been used for network characterization of signal magnitude. Then, with the expansion of network analysis technology, refinements were made to digital components such as ADCs (analog-to-digital converters), boosting the potential capabilities of these types of analyzers. As a result, VNAs (vector network analyzers) are now easily able to measure signal data for both vector (phase and magnitude) and scalar (magnitude only).

1.2.1 Scalar Network Analyzers

Scalar network analyzers (SNAs) are able to pick up a signal in broadband and change it into low-frequency alternating current (AC) or direct current (DC) as a means to measure the radio frequency (RF) signal strength. The hardware used for the measurements include thermoelectric components and diodes. The hardware employed in power detection and down-converting is generally easy to access and relatively inexpensive, which is a beneficial feature of SNAs. At the same time, the receiver should be re-optimized in order to obtain accurate power measurements across a range of frequencies, as the detectors almost always are broadband components. Because of this, frequency sweeps can be easily accomplished by sweeping the RF source frequency while taking the power measurements for single frequencies traces (N. Instrument, 2014).

Figure 1.1 illustrates how scalar analyzers perform S_{21}measurements, which is accomplished by using a signal source to constantly sweep certain frequency ranges. The figure shows that a reference detector is utilized in the sweep. However, if a reference detector is unavailable, the transmission coefficient S_{21} can be determined using the transmitted signal's power ratio either with or without a DUT (device under test). If this approach is adopted, two separate sweeps must be donein order to obtain proper characterization of the device. Conversely, when a reference detector is available, it can be used to formulate the transmission coefficient as the ratio of incident to transmitted power. Additionally, reflection measurements can be made using directional devices such as a bridge or a coupler shown in

Figure 1.1. In this case, the signal is detected by the DUT as a reflection, and the reflection coefficient is written as the reflected signal power's ratio over the incident signal power for a specific component or piece of equipment placed at the test port.

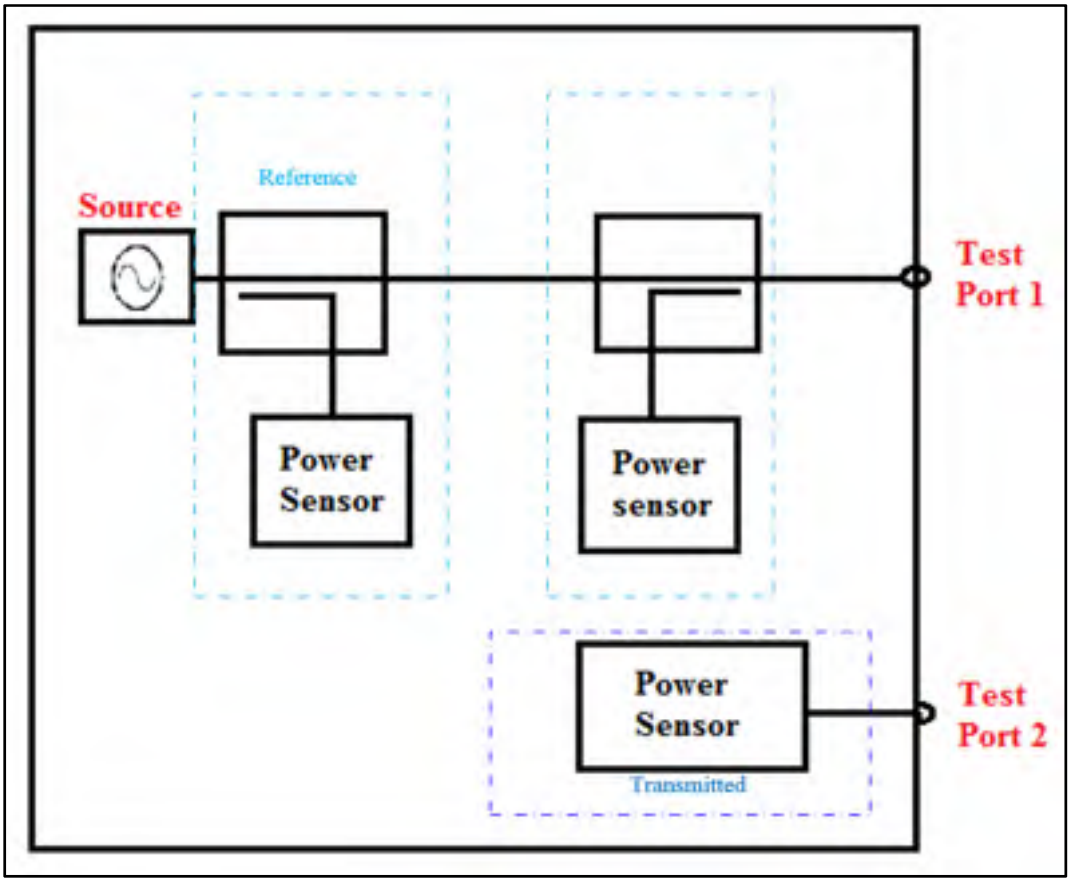

Figure 1.1Simplified depiction of scalar network analyzer (SNA).
After N. Instrument, 2014

As straightforward as these processes appear, SNAs are also known to experience measurement-related problems, including the intrusion of unwanted broadband noise. Furthermore, given the scalar aspect of the calibration, the test outcomes are relatively inaccurate compared to vector calibration. Moreover, the poor selectivity of SNAs means that they suffer from limitations to their dynamic ranges, whereas VNAs have much wider and less limited ranges. Finally, the use of couplers or bridges also leads to their relatively large size and bulkiness.

1.2.2 Vector Network Analyzers

Although more accurate in measurement detail and less limited in range than SNAs, vector network analyzers (VNAs) typically employ full heterodyne receivers in order to measure both signal magnitude and signal phase. As well, VNAs are much more complicated in design than SNAs, but the added complexity means that VNAs have the benefit of enhanced accuracy over SNAs. Specifically, in comparing VNAs to SNAs, the receiver's narrower bands can deal with unwanted broadband noise better, give a wider dynamic range, and employ error models that are more complex and therefore ultimately more accurate than models used in SNAs. The main disadvantage of VNAs is that the intricacies inherent in their heterodyne receiver architecture mean that the receivers must carry out frequency sweeps relatively slowly compared to broadband SNAs. This complexity also makes the technology much costlier than the other (K. Hoffmann and Z. Skvor, 1998).

As mentioned in earlier section, the main purpose of VNAs has traditionally been measuring phase and amplitude for reflected and incident waves positioned near DUT ports. Moreover, the VNA's relatively simplistic architecture enables it to be used for stimulating RF networks using signals from either a swept or stepped continuous wave (CW). VNAs are also designed for measuring travelling waves both near stimulus ports and along every port in the applied network that is terminated with 50- or 75-Ohm load impedances. Figure 1.2 depicts the main building blocks of a VNA (N. Instrument, 2014).

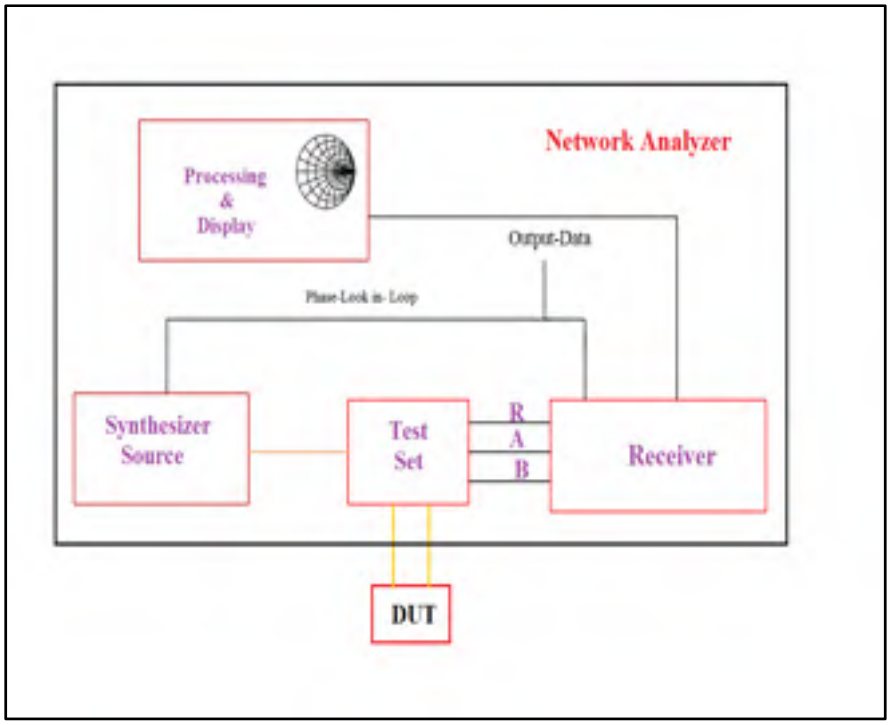

Figure 1.2Diagram of VNA main block

In the architecture of Figure 1.2, there is a synthesized RF source of Z_0 output impedance (characteristic/line impedances) along with three RF ports in the standard network analyzer. A sample of the source signal is measured using the reference port R (reference), while ports A and B measure the reflected and incident waves on the DUT. Two sequences (Tektronix, 2017)are needed for measuring the S-parameter matrices for a two-port network. The first sequence, illustrated in Figure 1.33, enables the measurement of the reflections at port 1, $S_{11}= {b_1}/{a_1}$, and the forward transmission from port 1 to port,$S_{21}= {b_2}/{a_1}$.The second sequence, illustrated in the sameFigure 1.3b, enables the measurement of the reflections at port 2, $S_{22}= {b_2}/{a_2}$, and the forward transmission from port 1 to port,$S_{12}= {b_1}/{a_2}$ where $a_1$and $a_2$are the forward waves and $b_1$and $b_2$are the backward waves.

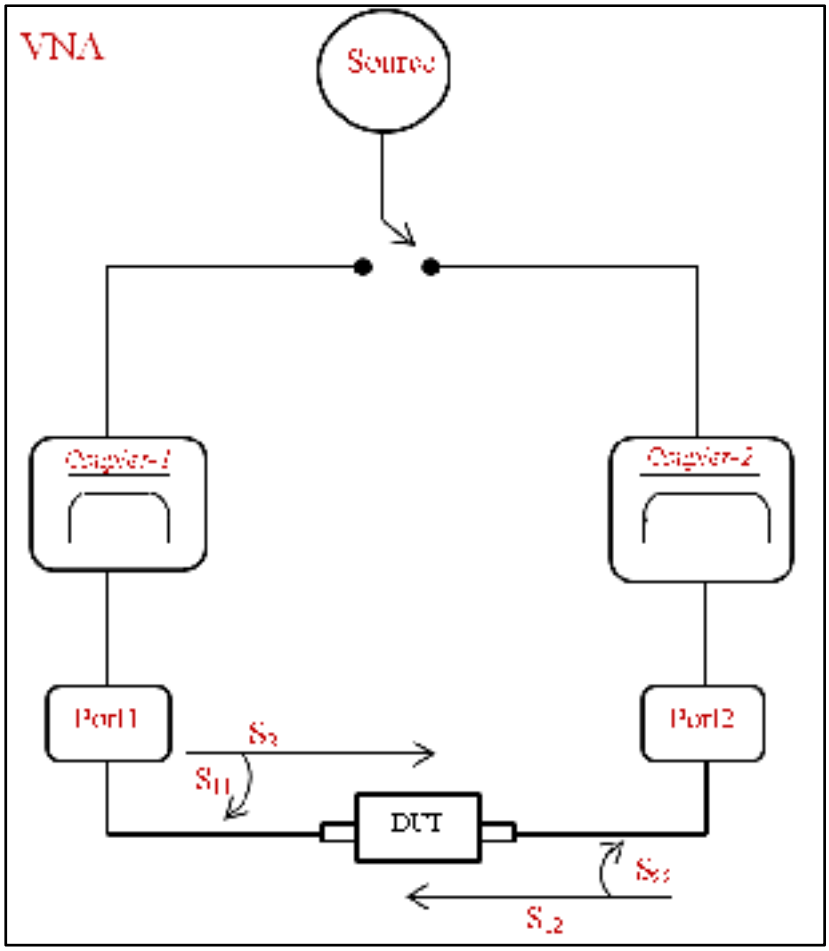

Figure 1.3Measurement of forward-scattering parameters witha network analyzer and reverse scattering parameters measurements obtained by network analyzer

VNA Calibration

The main reason for developing VNAs is making magnitude and phase measurements for reflected and incident waves. Thisis accomplished through precise characterization of a device's linear behavior. By obtaining magnitude and phase measurements from the waves, several different characteristics can be discovered concerning the device's features, such as insertion loss, return loss, group delay as well as impedance. From this, it can be seen that a VNA's precision in measuring a DUT's behavior depends on the precision of the magnitude and phase relationship measurement for incidentand/or reflected waves. VNAs can be calibrated during manufacturing for factors like receiver accuracy. However, details on the

measurement setup in the post-manufacturing phases are far more important for obtaining better measurement precision (N. Instrument, 2014).

There is much impairment which can hinder VNAs in making precise network analysis measurements, so calibration should be used first to measure the impairments individually and then to adjust the measurement results accordingly. Numerous approaches can be employed for VNA calibration. Which is the most appropriate method depends on a variety of factors, such as available calibration standards, frequency range, port number, and DUT port type. For instance, a VNA port type may be wave guide, in fixture, on wafer, or co-axial. Another major VNA calibration type differentiation involves the trade-off between speed and precision. Calibrating a two-port, full S-parameter VNA is typically done using one of the following three methods: full S-parameter calibration; one-path, two-port calibration; or frequency response calibration.

1.3 Six-Port Techniques

The most essential problem in microwave engineering and wireless communications system is to have a design with high performance and low cost measurement techniques. Thus, six-port technique that will be reviewed in this section allows determining the efficient of the system or network.

1.3.1 Overview

The six-port method, which has undergone continuous development and improvements, was introduced as a measurement technique by Engen and Hoer in 1970s to determine the amplitude and phase of RF signals based on four scalar power readings (F. M. Ghannouchi, A. Mohammadi, 2009). A six-port junction is the essential part of the six-port technique that is well-suited for low-complexity network analyzer tasks as an alternative to conventional VNAs. Figure 1.4 shows a typical six-port junction which contains two directional couplers to sample the incident and reflected waves (D1, D2), five power dividers (PD1 – PD5) a and hybrid coupler (Q).Four power detectors connected to ports 3 to 6 are used to measurefour

magnitudes that help in computing the complex reflection coefficient value for the device under test DUT (Y. Cassivi, and al, 1992).

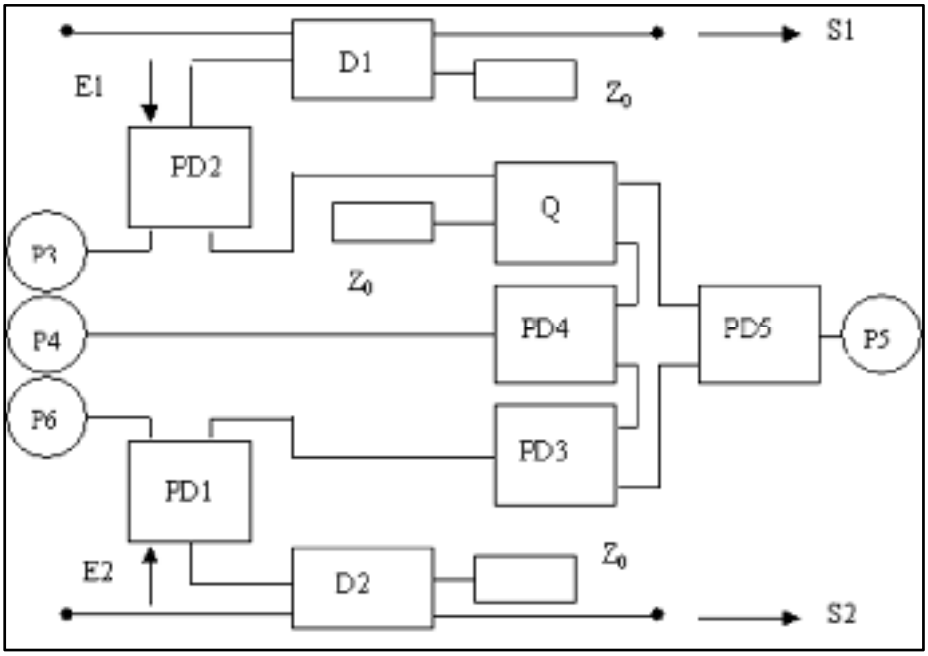

Figure 1.4Six-port junction diagram
taken from Y. Cassivi, and al(1992, p.465)

Because of the need to decrease the costof digital transceivers, several direct-conversion transceivers which used six-port technology are proposed in(C. A. Hoer, 1972), where simple techniques are usedfor measuring voltage, current, power, complex impedance, and phase angle utilizing a six-port coupler. The four side arms of this ideal six-port have output voltages proportional to the voltage as presented in Figure 1.5, current, incident voltage wave, and reflected voltage wave, respectively, all referred to some desired reference plane in the transmission line.

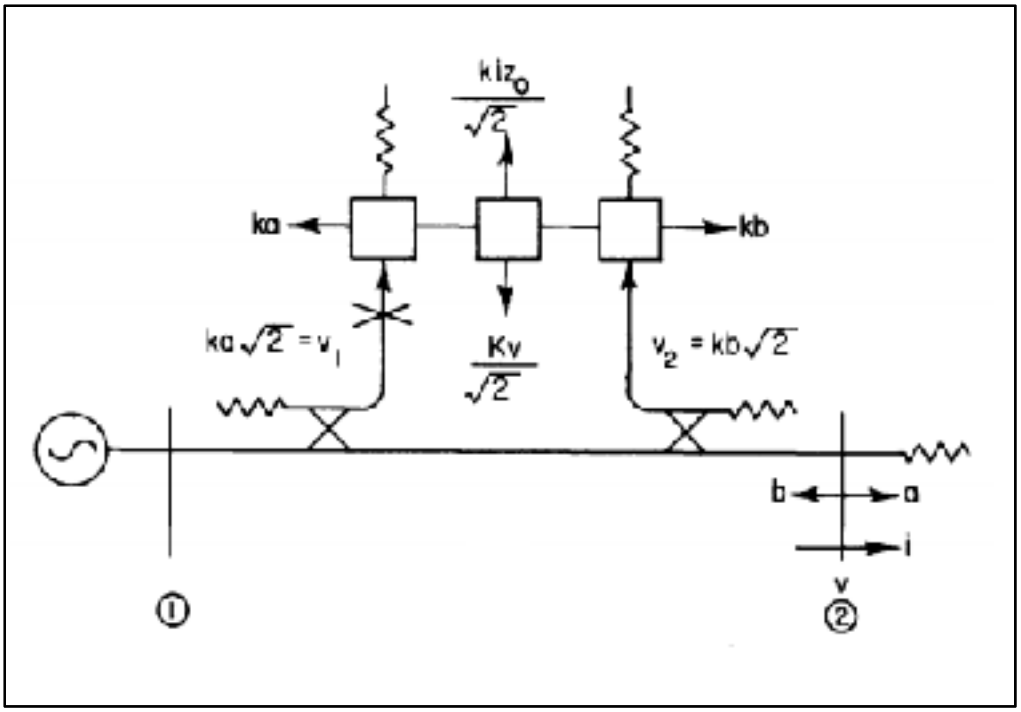

Figure 1.5Utilizing ideal hybrids, couplers, and voltage and current probes
taken from C. A. Hoer(1972, p.468)

In (G. F. Engen and C. A. Hoer,1972), a six-port homodyne method employed power detectors rather than mixers as in Figure 1.6, resulting in less complex circuits compared to the traditional six-port heterodyne approach. The benefits of using the six-port homodyne receiver include ultra-low power consumption, less costly transceivers, and easily obtained broadband specifications from passive elements.

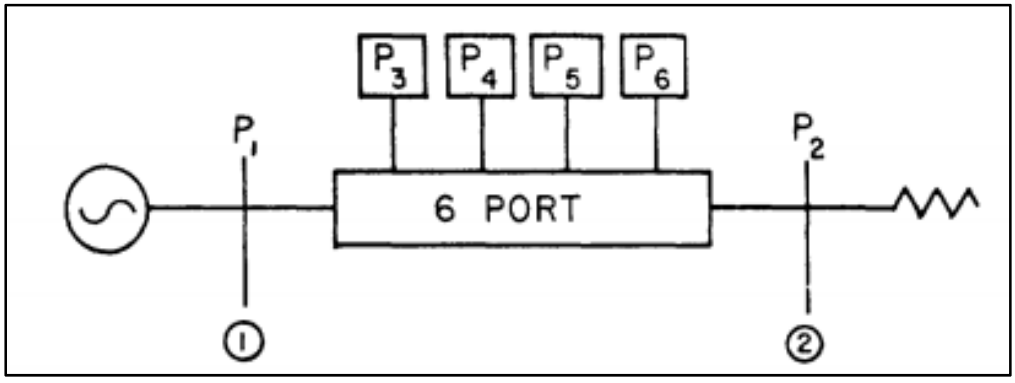

Figure 1.6Arbitrary six-port junction representation
taken from G. F. Engen and C. A. Hoer(1972, p.471)

The RF circuit's ultra-large frequency bandwidth is a crucial benefit of six-port design and the main reason why, in six-port transceiver architectures, it is used in applications such as ultra-wideband (UWB) systems and software-defined radio (C. A. Hoer,1977),the latest wireless applications. In (E. R. B. Hansson, G. P. Riblet, 1983), the researchers used a six-port transceiver at 60 GHz in CMOS technology, intending to develop a low-cost, low DC power-consuming miniature transceiver. The proposed transceiver in (E. R. B. Hansson, G. P. Riblet, 1983) showed total DC power consumption under 100 mW.

A new automobile radar based on the six-port phase/frequency discriminator where the block diagram of the proposed prototype as in Figure 1.7 includes microwave oscillator, modulator and the VCO, the six-port, which plays the role of a mixer., and power detectors are placed at outputs 3–6. The frequency of the four signals that go into the analog–to–digital (A/D) converter is the Doppler frequency of the target. This technique forces the modulation frequency to be the half of the sampling to ensure the Nyquist theorem; the sampling frequency should be at least the double of the highest frequency that is expected to measure (C. Gutierrez Miguelez, and al,2000).

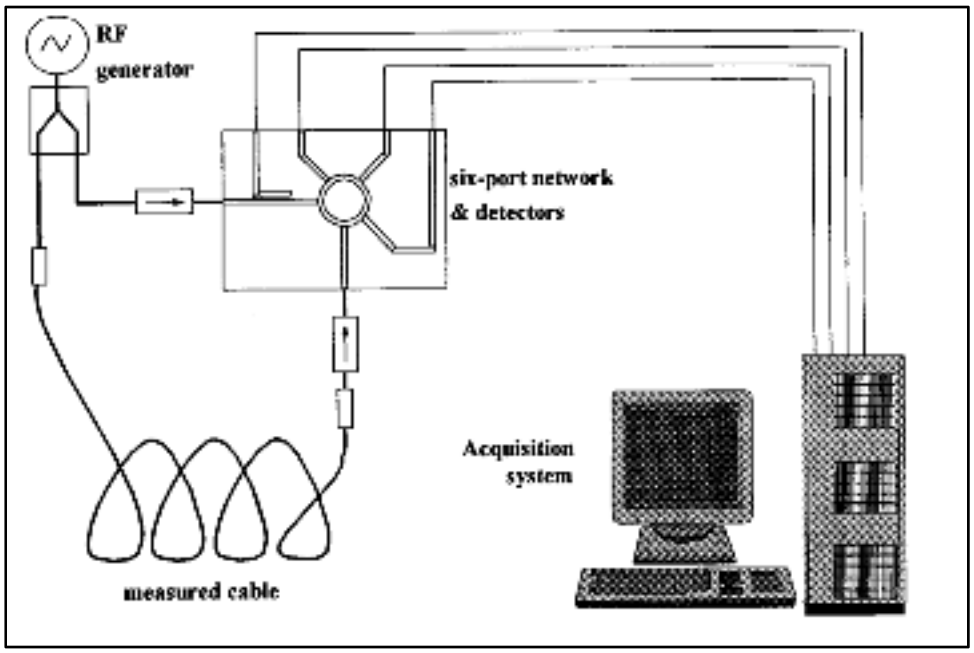

Figure 1.7Block diagram of the proposed radar
taken from C. Gutierrez Miguelez (2000, p.1417)

1.3.2 The Six-Port Reflectometer

A six-port reflectometer is a passive microwave six-port junction that allows the measurement of the complex reflection coefficient ratio of two RF signals using four power detector circuits (D_3, D_4, D_5, D_6) only, (G. F. Engen,1977).Figure 1.8 illustrates a block diagram of a six-port reflectometer with a source connected at port 1 and the DUT connected at port 2.

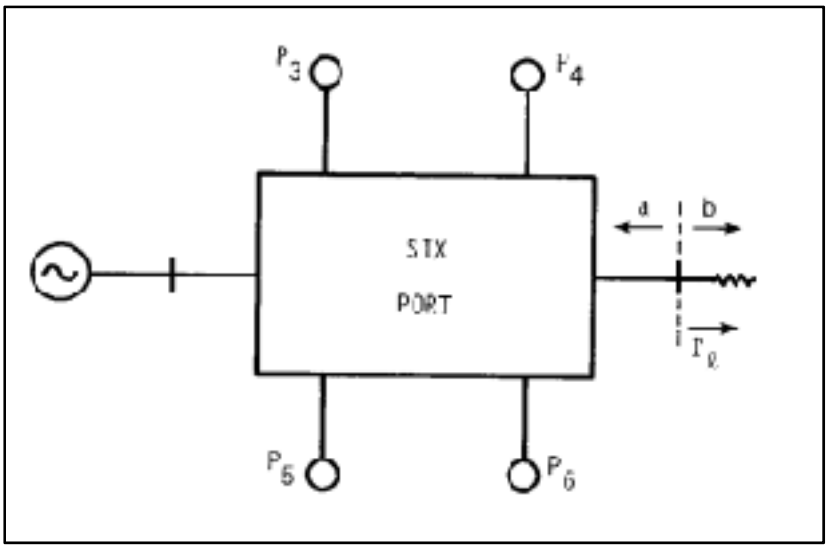

Figure 1.8Block diagram of six-port reflectometer
taken from G. F. Engen(1977, p.44).

The powers detected at ports P3-P6 are formulated in terms of reflected (b_2) and forward (a_2) waves as follows (G. F. Engen,1977):

$$P_3 = |A * a_2 + B * b_2|^2 \quad (1.1)$$

$$P_4 = |C * a_2 + D * b_2|^2 \quad (1.2)$$

$$P_5 = |E * a_2 + F * b_2|^2 \quad (1.3)$$

$$P_6 = |G * a_2 + H * b_2|^2 \quad (1.4)$$

where A, B, C, D, E, F, G and H are complex constants specific to the six-port junction. Equations 1.1 to 1.4 can be reformulated in terms of the reflected power,$|b_2|^2$, and the unknown load reflection coefficient$\Gamma_L$as:

$$P_3 = |A|^2 |b_2|^2 \ |\Gamma_L - q_3|^2 \tag{1.5}$$

$$P_4 = |C|^2 |b_2|^2 \ |\Gamma_L - q_4|^2 \tag{1.6}$$

$$P_5 = |E|^2 |b_2|^2 \ |\Gamma_L - q_5|^2 \tag{1.7}$$

$$P_6 = |G|^2 |b_2|^2 \ |\Gamma_L - q_6|^2 \tag{1.8}$$

where: q_3=-B/A, q_4=-D/C, q_5=-F/E, q_6=-H/G.

In (G. F. Engen,1977), Engen introduced a design where port 3 is used as a reference port and is coupled to the reflectometer's port 1 directly. Port 1, being the injection site for input power, is insensitive to port 2, being the origin of the reflected wave. Under these conditions, Equation 1.1 becomes:

$$P_3 = | B * b_2|^2 \tag{1.9}$$

Using thepower at port 3 as a reference power to find the reflection coefficient, the powers (i.e., power ratios) at the other ports are normalized as follows: P_4/P_3, P_5/P_3, and P_6/P_3. Based on this, we obtain the following equations:

$$\frac{P_4}{P_3} = \frac{|\Gamma_L - q_4|^2}{|\frac{B}{C}|^2} \tag{1.10}$$

$$\frac{P_5}{P_3} = \frac{|\Gamma_L - q_5|^2}{|\frac{B}{E}|^2} \tag{1.11}$$

$$\frac{P_6}{P_3} = \frac{|\Gamma_L - q_6|^2}{|\frac{B}{G}|^2} \tag{1.12}$$

In this form, it is clear that the 'q' points in Equations 1.10 to 1.12are the centres for three circles in the complex plane. If we define the radii of these circles as R_4, R_5 and R_6, then these equations can be re-written as:

$$R_4 = |\Gamma_L - q_4| \tag{1.13}$$

$$R_5 = |\Gamma_L - q_5| \tag{1.14}$$

$$R_6 = |\Gamma_L - q_6| \tag{1.15}$$

The unknown load reflection coefficient, Γ_L, is then found by the intersection of these three circles as illustrated in Figure 1.9.

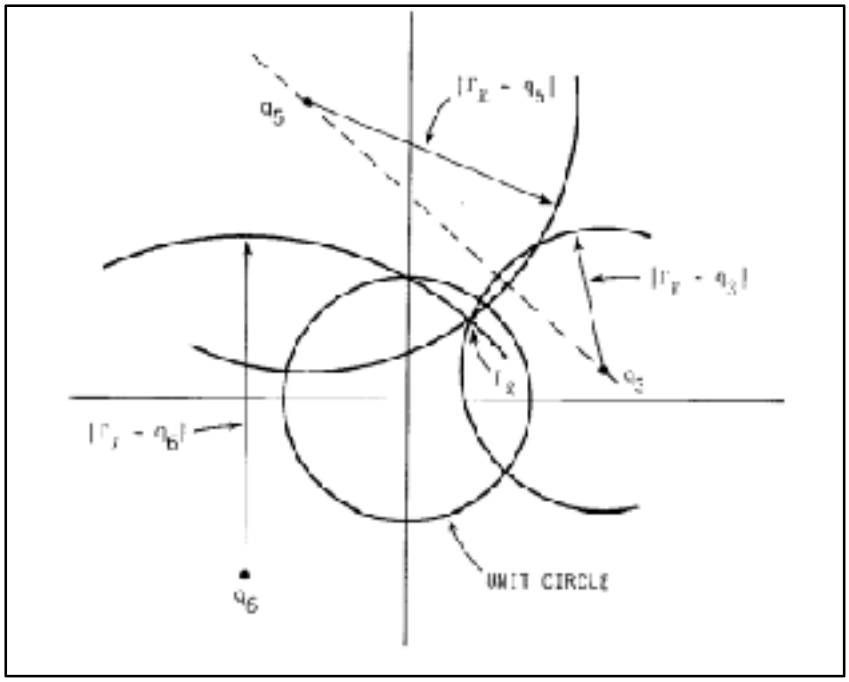

Figure 1.9Geometric impact of Equations1.10 – 1.15
in formulatingcomplex reflection coefficients
taken from G. F. Engen(1977, p.46)

By employing added detectors, the six-port approach can give a more cost-effective measurement for both phase and amplitude. At the same time, the six-port method can also provide more accurate power measurements as well as network parameters. Using the six-port method enables impedance and power flow measurements to be performed at the same time by utilizing the amplitude measurements (i.e., no need for phase measurements). Additionally, as demonstrated in (A. L. Samuel,1974), if one or two six-port configurations is/are used along with a suitable calibration and test-set strategy, they can measure the four scattering parameters for two-port DUTs. The six-point design can also be used for directional finding of received waveforms (A. Koelpin, al,2010). Other applications of the six-port technology are polarization and near-field antenna measurement and in the radar system, giving the desired high performance/low cost in lucrative fields such as the automotive industry (C. Nieh, T. Huang, and J. Lin,2014).

1.4 Phase and Gain Detection

Dedicated gain and phase detection circuits offer another alternative solution for measuring the amplitude and phase of two RF signals. The AD8302 from Analog Devices (Analog Devices, 2002) is one such circuit that includes demodulating logarithmic amplifiers with 60 dB dynamic range as shown in Figure 1.10. So, by taking the difference between their outputs OFSA and OFSB, the magnitude ratio or gain between the input signals (INPA and INPB) can be gained. Further, it contains a phase detector of multiplier kind. The phase accuracy is not dependentof the level of signal over the large range. The AD8302 issues two voltages at the outputs VMAG and VPHS that are corresponding to the differences of gain and phase between the two measured branches. The practical block diagram of the AD8302 present in Figure 1.10 bellow:

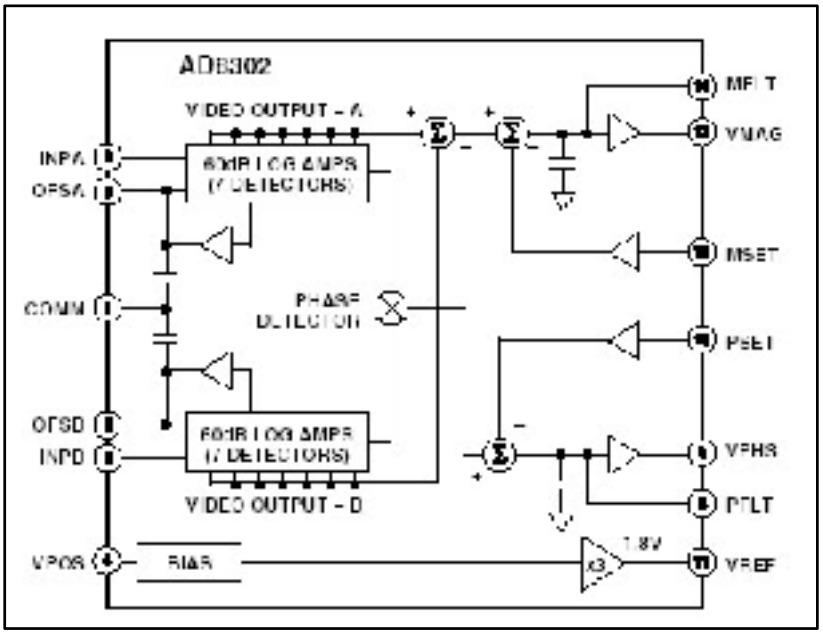

Figure 1.10Functional photograph of the AD8302
taken from Analog Devices data sheet(2002, p.1)

It should be noted that the AD8302 requires the use the directional couplers to sample the waves, which increases the size and losses. Moreover, calibration at one of the inputs (INPA or INPB)as ACreference signalis requiredbefore carrying out measurements.

1.5 Conclusion

This chapter presented different microwave scalar and vector measurement techniques. Starting from the best known technique widely used to measure the relative amplitude and phase of RF signal is vector network analyzer VNA. This VNA provides very high accuracyand wideband measurement over the frequency range. Because of the complexity of vector network analyzer, the six-port junction is an alternative technique that reduces the complexity of the measurements and provides the vector measurement by using couplers, dividers, mixers, and power detector circuits and other microwave components. Further, six-port technique reduces the complexity of six-port junction by using only couplers and power detector circuits as well as Gain and Phase detection circuit with 60 dB dynamic range. Despite all the advantages of these techniques; from accurate measurement and wide frequency range, all of these approaches are use the directional coupler for sampling reflected and incident waves. Due to size issues with the coupler, integrating it into an embedded system is impractical, especially at low frequencies. Moreover, this architecture would demand additional calibration efforts and necessitate a directional coupler and multiple dividers/hybrids, again making the design unsuitable for current and future needs and trends.

CHAPTER 2

PROPOSED REFLECTOMETER

Chapter 1 presented different alternative techniques for RF vector measurements using the directional couplers, which have the disadvantages of large size making them not suitable for circuit integration and embedded measurement. In this chapter, an alternative technique that is suitable for circuit integration and embedded measurement using a four-port reflectometer will be presented. The new optimized four port reflectometer will be descried and the theory for computing the reflection coefficient of the device under tests DUTs will be presented.

2.1 Related Work

In 2010, a novel design of four-port reflectometer was investigated(A. B. Kouki, et al., 2010). The reflectometer, see Figure 2.1, used (i) a microstripline (Signal-carrying line),where the RF source is connected at the input (port 1) and the device under test is connected to the output (port 2) of this signal-carrying line, (ii) two sniffers located close to the transmission line on the same layer and separated by the distance d, and (iii) two power detector circuits linked to the coupled ports 3 and 4 to measure the coupled power.

Basically, the sniffers are very simple structures that have very small size and provide very low coupling (below -30 dB). This makes the reflectometer more convenient for integration in microwave circuits to enable embedded measurement. Because of having a very low coupling factor, the sniffers will not have any effect on the propagation of the power signal in the system. However, having the sniffers in the shown planner arrangement, i.e., close to the signal-carrying traces, will impose restrictions on the circuit design and the routing of additional traces.

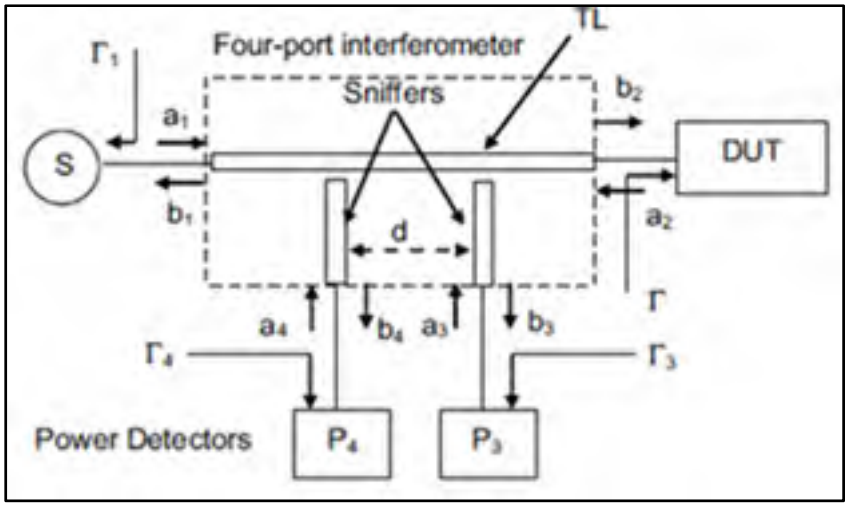

Figure 2.1Four-port reflectometer topology
Taken from A. B. Kouki, et al., (2010, p.2)

2.2 Proposed 3D Four-Port Reflectometer Description

To avoid the above-mentioned limitations explicitly, the sniffer lines must be designed so that they do not intersect other signal lines. To accomplish this, we proposed to perform signal sniffing differently. The proposed reflectometer uses new sniffers which are made of partially filled vertical vias in 3D placed under the signal carrying transmission line. In this manner, the surface of the circuit is freed from any complex routing of lines. Furthermore, these sniffers offereven more size reduction and are very well suited for circuit integration and embedded measurement.

Figure 2.2 illustrates the proposed structure where port 1 of the transmission line is connected to the RF input power while port 2 of the transmission serves to connect the DUT. Thetwo sniffers are placed a distance d apart underneath of the transmission line in a 3D form to couple very small portions(-30 dB) of the companied forward and backward signals. These sniffers are connected to two power detector circuits, LT5582 (Analog Devices, 2010-2018),for power measurement at ports 3 and 4 through a buried line.To route the sniffed signals to the surface of the circuit at its edges, transitions are needed. The design of these transitions uses vertical vias as shown in Figure 2.3 which are typically highly inductive.

Therefore, careful compensation of these transitions is required to keep a matched impedance from the sniffers to the surface lines.

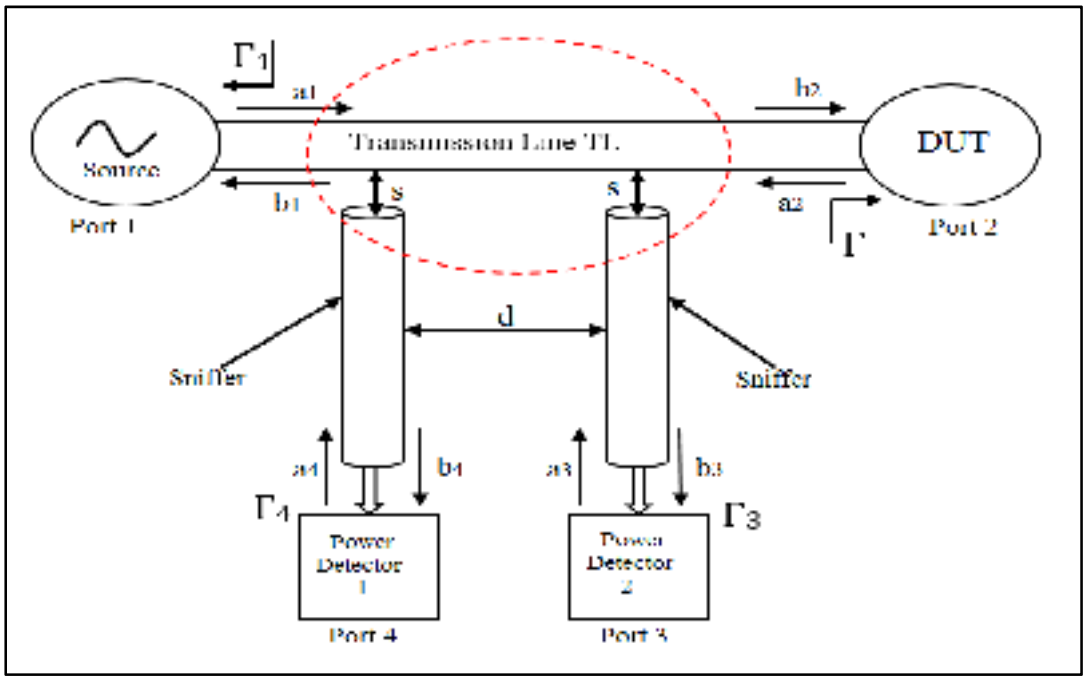

Figure 2.2The block diagram of proposed 3D four-port reflectometer

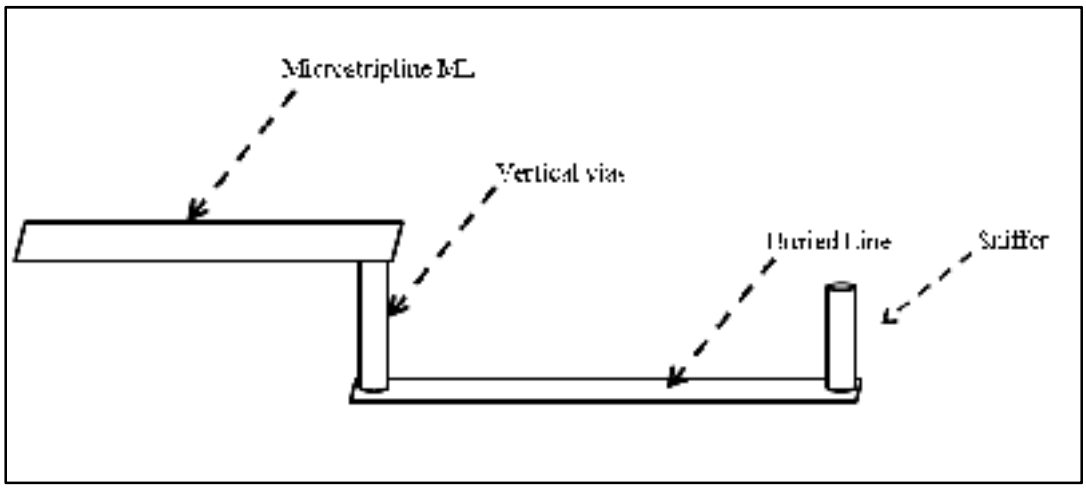

Figure 2.3Buried line to microstripline vertical transition.

2.3 Reflection Coefficient Determination

First, we assume that the S-parameters of the reflectometer are known. This can be accomplished by 3D field simulation of the reflectometer geometry or from measurement of the fabricated reflectometer prototype. Referring to Figure 2.1, the reflection coefficient of the DUT at port 2 is given by:

$$\Gamma_L = \frac{a_2}{b_2} \tag{2.1}$$

Further, the measured powers at ports 3 and 4 are given in terms of the waves b_3 and b_4 as follows (assuming well matched ports):

$$P_3 = \left|b_3\right|^2 \tag{2.2}$$

$$P_4 = \left|b_4\right|^2 \tag{2.3}$$

Next, we determine the transmission coefficients from port 1 to port 3, T_{31}, and to port 4, T_{41}. Using signal flow graph analysis and Mason's rule (G. Gonzales, 1977), (A. B. Kouki, et al., 2010) the following expressions in terms of the reflectometer's S-parameters can be obtained:

$$T_{31} = \frac{b_3}{a_1} = S_{31} + \frac{S_{32}S_{21}\Gamma_L}{1 - S_{22}\Gamma_L} = \frac{(S_{32}S_{21} - S_{31}S_{22})\Gamma_L + S_{31}}{-S_{22}\Gamma_L + 1}, \text{ where } a_3, a_4 = 0 \tag{2.4}$$

$$T_{41} = \frac{b_4}{a_1} = S_{41} + \frac{S_{42}S_{21}\Gamma_L}{1 - S_{22}\Gamma_L} = \frac{(S_{42}S_{21} - S_{41}S_{22})\Gamma_L + S_{41}}{-S_{22}\Gamma_L + 1}, \text{ where } a_3, a_4 = 0 \tag{2.5}$$

The S-parameters in the equations (2.4) and (2.5) can be grouped using six new variables, A_1, A_2, B_1, B_2, C, and D as:

$$\begin{bmatrix} A_1 & A_2 \\ B_1 & B_2 \\ C & D \end{bmatrix} = \begin{bmatrix} (S_{21}S_{32} - S_{31}S_{22}) & (S_{21}S_{42} - S_{41}S_{22}) \\ S_{31} & S_{41} \\ -S_{22} & 1 \end{bmatrix} \tag{2.6}$$

Then T_{31} and T_{41} can be rewritten explicitly in terms of these known new variables and the unknown DUT's reflection coefficient as:

$$T_{31} = \frac{b_3}{a_1} = \frac{1}{a_1} X \frac{A_1\Gamma_L + B_1}{C\Gamma_L + D} \tag{2.7}$$

$$T_{41} = \frac{b_4}{a_1} = \frac{1}{a_1} X \frac{A_2\Gamma_L + B_2}{C\Gamma_L + D} \tag{2.8}$$

By using equations (2.7) and (2.8) in equations (2.2) and (2.3), the measured power at ports 3 and 4 can be written as:

$$P_3 = P_1 \left| \frac{A_1\Gamma_L + B_1}{C\Gamma_L + D} \right|^2 \tag{2.9}$$

$$P_4 = P_1 \left| \frac{A_2\Gamma_L + B_2}{C\Gamma_L + D} \right|^2 \tag{2.10}$$

where P_1 is the input power at port 1 ($P_1 = |a_1|^2$).

Writing $\Gamma_L = x+jy$, equations (2.9) and (2.10) can be written as:

$$(x-\alpha_3)^2+(y-\beta_3)^2=r_3^2 \tag{2.11}$$

$$(x-\alpha_4)^2+(y-\beta_4)^2=r_4^2 \tag{2.12}$$

whereα_3, β_3, α_4, β_4,r_3, and r_4 are six complex parameters which are expressed interms of A_1, B_1, A_2, B_2, C, D, and P_1, all known quantities. These parameters are given by:

$$\alpha_3=-\left(\frac{(D_rC_r+D_iC_i)P_{31}-(B_{1r}A_{1r}+B_{1i}A_{1i})}{P_{31}(C_r^2+C_i^2)-(A_{1r}^2+A_{1i}^2)}\right), \tag{2.13}$$

$$\beta_3=-\left(\frac{(D_iC_r-D_rC_i)P_{31}-(B_{1i}A_{1r}-B_{1r}A_{1i})}{P_{31}(C_r^2+C_i^2)-(A_{1r}^2+A_{1i}^2)}\right), \tag{2.14}$$

$$r_3=sqrt\left(\frac{(B_{1i}^2+B_{1r}^2)-(D_r^2+D_i^2)P_{31}}{P_{31}(C_r^2+C_i^2)-(A_{1r}^2+A_{1i}^2)+\alpha_3^2+\beta_3^2}\right), \tag{2.15}$$

$$\alpha_4=-\left(\frac{(D_rC_r+D_iC_i)P_{41}-(B_{2r}A_{2r}+B_{2i}A_{2i})}{P_{41}(C_r^2+C_i^2)-(A_{2r}^2+A_{2i}^2)}\right), \tag{2.16}$$

$$\beta_4=-\left(\frac{(D_tC_r-D_rC_i)P_{41}-(B_{2i}A_{2r}-B_{2r}A_{2i})}{P_{41}(C_r^2+C_i^2)-(A_{2r}^2+A_{2i}^2)}\right), \tag{2.17}$$

$$r_4 = sqrt\left(\frac{(B_{2i}^2 + B_{2r}^2) - (D_r^2 + D_i^2)P_{41}}{P_{41}(C_r^2 + C_i^2) - (A_{2r}^2 + A_{2i}^2) + \alpha_4^2 + \beta_4^2}\right), \tag{2.18}$$

Equations (2.11) and (2.12) represent two circles in the complex plane centered at $Q_3$of coordinates (α_3, β_3) and $Q_4$of coordinates (α_4, β_4) and or radii r_3 and r_4, respectively. The solution to these equations can be found graphically by finding the intersection between the two circles as shown in Figure 2.4. The existence and the positionsof the two intersecting points depend on the distance d that is separating the two sniffers. Additionally, of the two intersections one will be inside the unit circle on complex Γ plane while the other one will be outside of the circle as seen in Figure 2.4. For passive loads, the following condition must be met, which means that only the intersection point inside the unit circle is retained as a solution:

$$\left|\Gamma_L\right|^2 = x^2 + y^2 \leq 1 \tag{2.19}$$

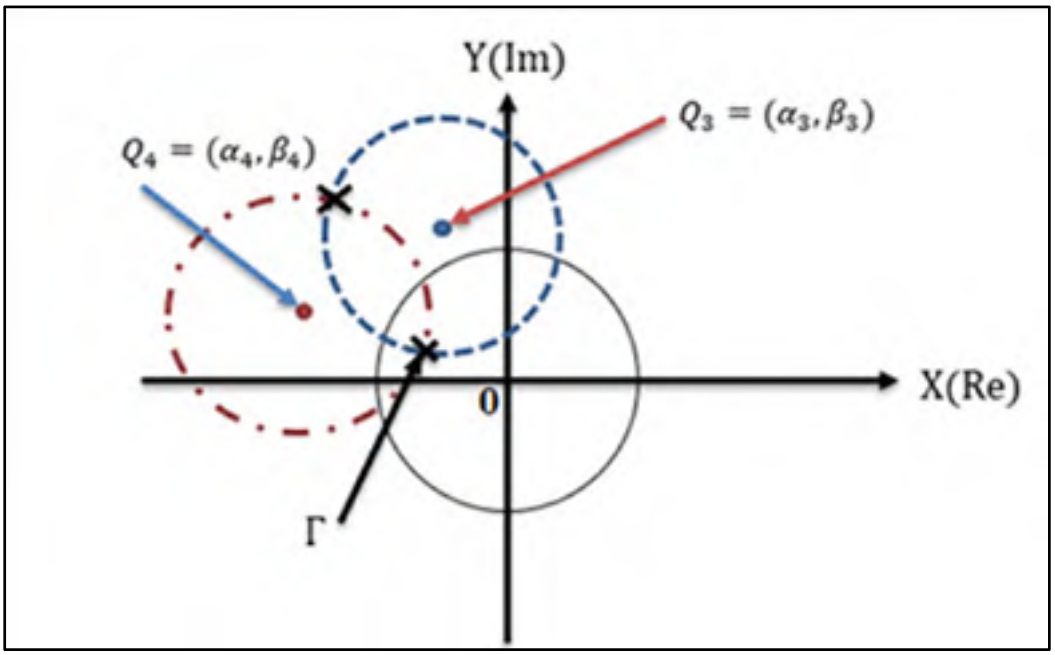

Figure 2.4Two circles intersection in the complex plane todefine the reflection coefficient (Γ)

CHAPTER 3

PROPOSED REFLECTOMETER

In this chapter, the proposed 3D four-port reflectometer will be implemented. The frequency of operation is chosen to be 1.2 GHz. The reflectometeris first simulated using a 3D electromagnetic field simulator HFSS and later fabricated in low temperature co-fired ceramics (LTCC) using four layers of Ferro L8 substrate as seen in Figure 3.1. Table 1 summarizes the main characteristics of the substrate used.

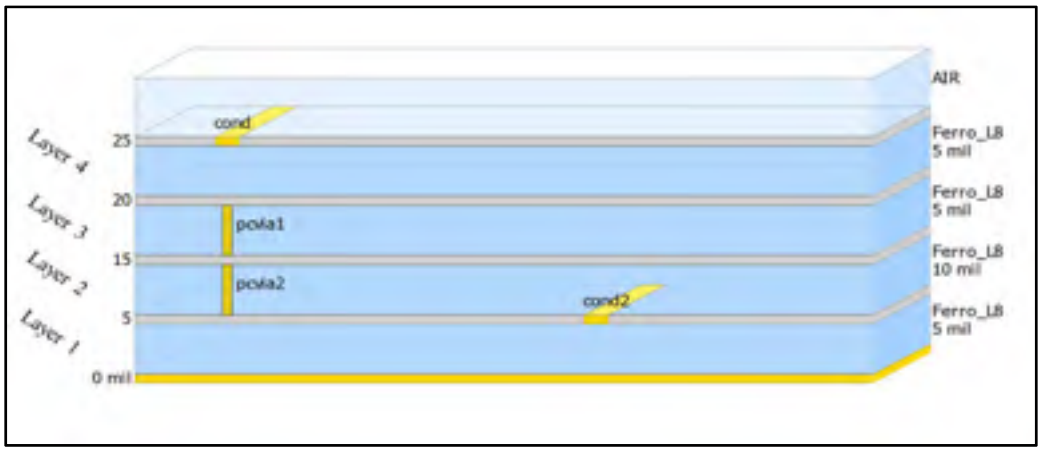

Figure 3.1illustrates the details of the stack of layers used throughout this chapter.

Table 3.1Ferro L8 characteristics

Parameters	Values
Dielectric Constant	7.2
Loss tangent	0.002 @ 1.2 GHz
Substrate thickness (before firing)	635 um

3.1 Microstripline Design and Simulation

First, a microstripline will be designed to connect the source at port 1 and the device under test at port 2. Itswidth (W), as shown in Figure 3.2, can be calculated using the formulas in (David M. Pozar, 2011) below:

(3.1)

where:

$$A = \frac{Z_0}{60}\sqrt{\frac{\varepsilon_r + 1}{2}} + \frac{\varepsilon_r - 1}{\varepsilon_r + 1}\left(0.23 + \frac{0.11}{\varepsilon_r}\right) \tag{3.2}$$

$$B = \frac{377\pi}{2Z_0\sqrt{\varepsilon_r}} \tag{3.3}$$

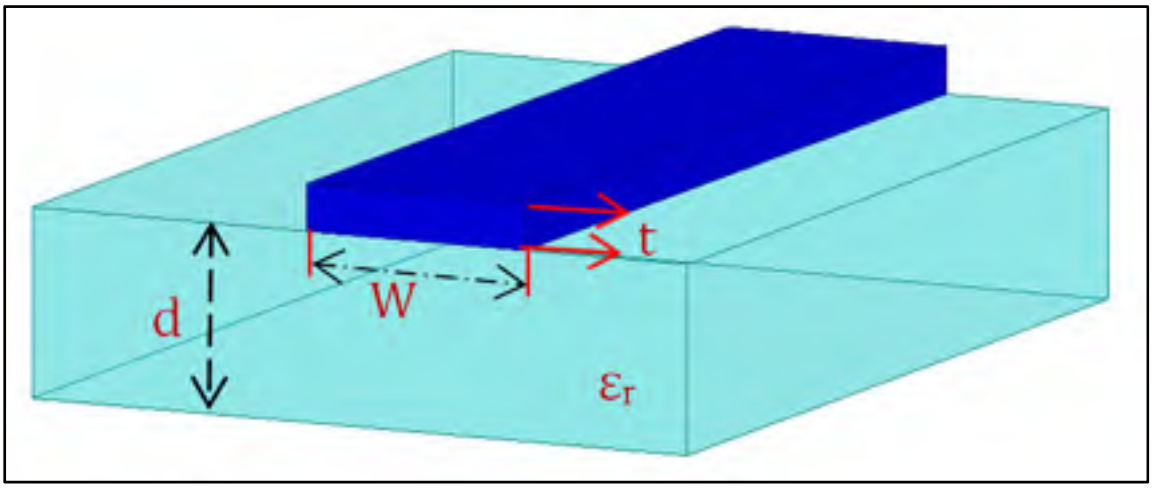

Figure 3.2Photograph of a microstripline structure

However, instead of using the above equations, the LineCalc tool in Advanced Design System ADS, see Figure 3.3, is used to compute the dimensions of a 50 Ω transmission line (Width, Length) on the Ferro L8 substrate with the characteristics given in Table 3.1.

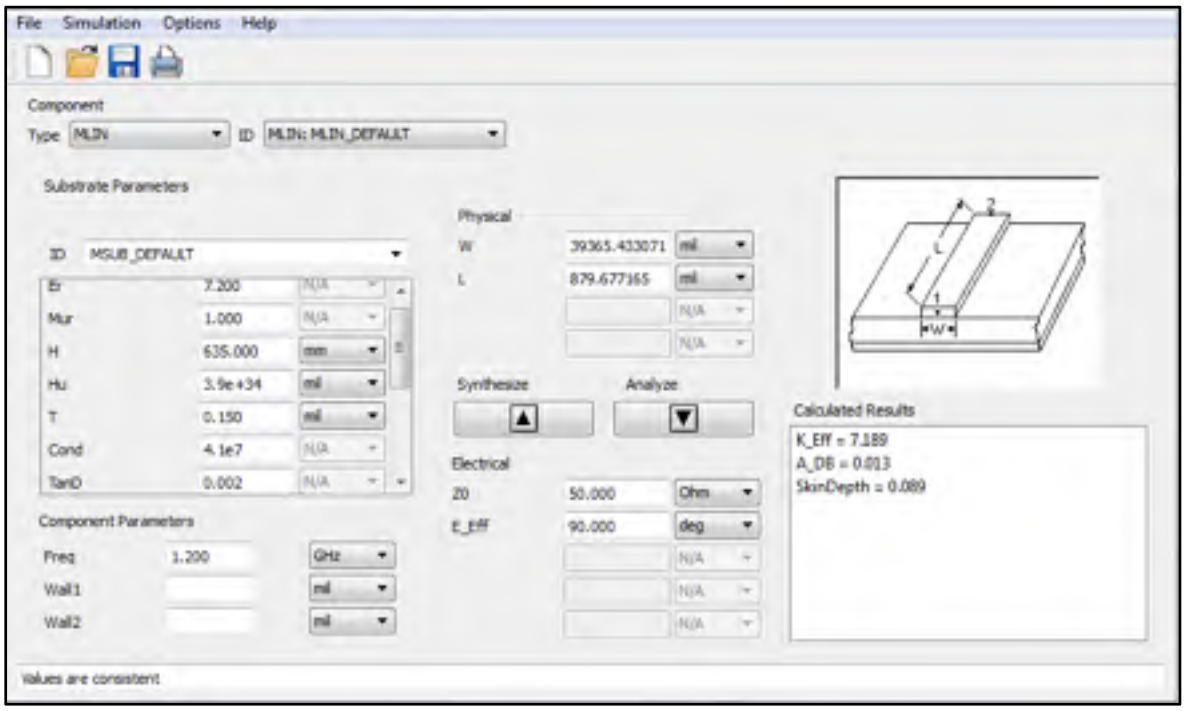

Figure 3.3LineCalc calculator layout

Once the microstripline is dimensioned, we built its 3D model for simulation. Figure 3.4 shows the designed microstripline in the3D high frequency simulator system HFSS, which is 3D electromagnetic simulation. The dimensions used are: 853 um in width and a length of 15 mm with a substrate thickness of 653 um. The first HFSS simulations confirm that this line is indeed a 50 Ω line. The next step is to introduce the sniffers under this transmission line in a 3D structure. This will be detailed in the following section.

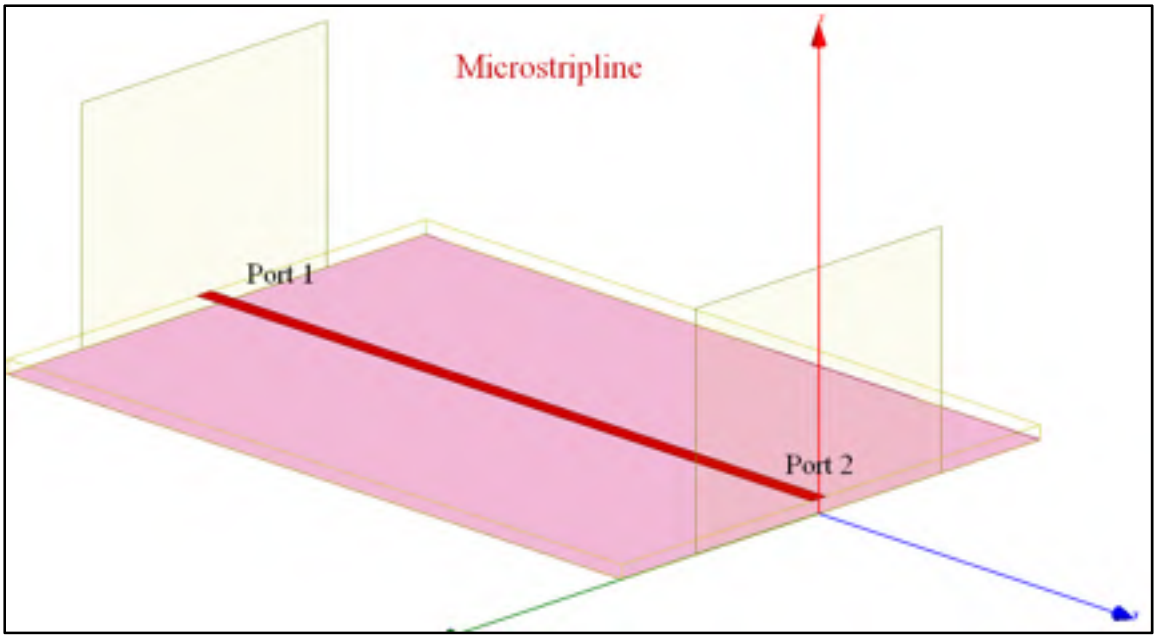

Figure 3.4Microstripline design in HFSS.

3.2 Sniffer Design

The aim of using sniffers, as explained in chapter 2, is to couple a small portion of the incident and reflected signals' power in order to measure the reflection coefficient of the device under test. These sniffers could be in different shapes and at different positions, like planner sniffers in (A. B. Kouki, et al., 2010) where the sniffers were located close to the transmission line TL on top of the substrate. Similarly, they could be close under the transmission line in a vertical position through the LTCC layers as we propose to do in our 3D reflectometerdesign. This can be achieved by using vias that are filled in several layers beneath the line without touching it. Cylindrical and rectangular vias are two kinds of vias that can be easily used to this end. Both types were simulated and their performance was found to be comparable. The diameter of the cylindrical via was 136.8 um while the rectangular vias measured 144.8um x 88.9 um, as shown in Figure 3.5. The viaswere centered under the microstripline with a vertical spacing of 127 um, which corresponds to the thickness of one layer. The coupling level was found to be -30 dB.As expected, it was found that the vertical spacing between the sniffer (vias) and the microstripline determines the amount of coupling that can be achieved. Therefore, depending on how much signal coupling

is needed, the thickness and number of layers that do not include vias can be adjusted to meet the desired coupling level.

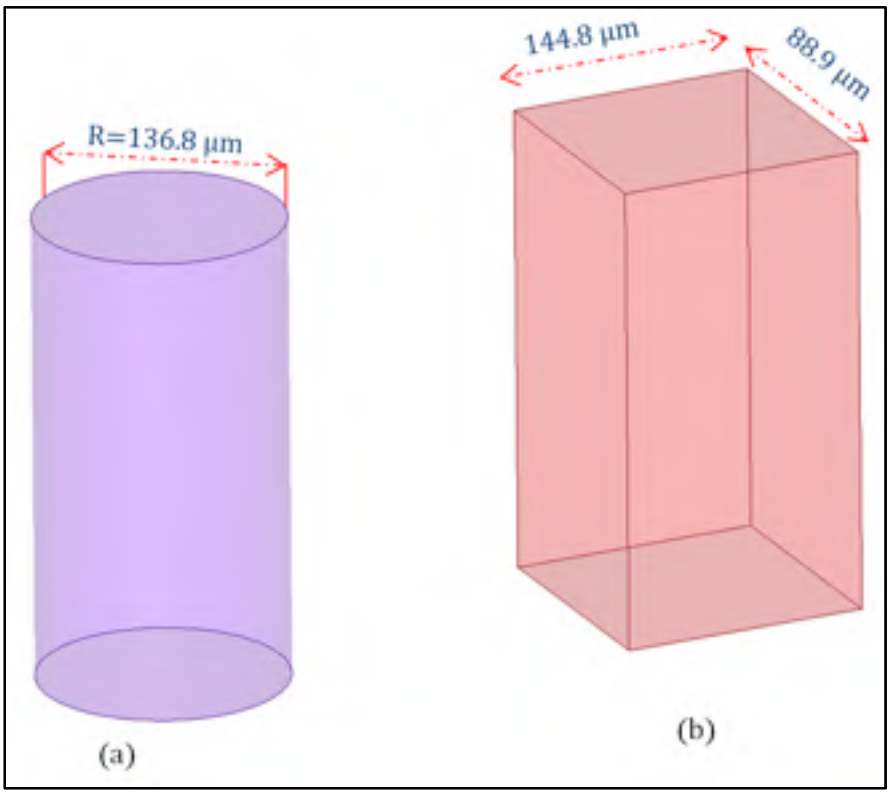

Figure 3.5(a) cylindrecal via (b) rectangular via

To route the sniffed signals from underneath the microstripline to the surface of the circuit where power detectors can be mounted, a buried transmission line with a transition to the surface of the circuit are needed. These must be carefully designed to maintain good impedance matching.

3.3 Perpendicular Transition Design

Figure 3.6 illustrates the geometry of the proposed transition design. It consists of a buried line (SL) connected to a surface microstrip line (ML) through a center via of 150 um diameter. The characteristic impedance of the buried line can easily be controlled by its width and does not pose a challenge in the design. However, the center via being much

smaller in diameter that the MS line width will introduce an inductive discontinuity that will cause impedance mismatch at the power detection ports. Therefore, this discontinuity must be compensated through the use of the additional grounded vias that surround the center via. All grounded vias have a diameter of 150 um. This structure approximates a vertical coaxial line whose characteristic impedance can be tuned by controlling the distance between the grounded and center vias.

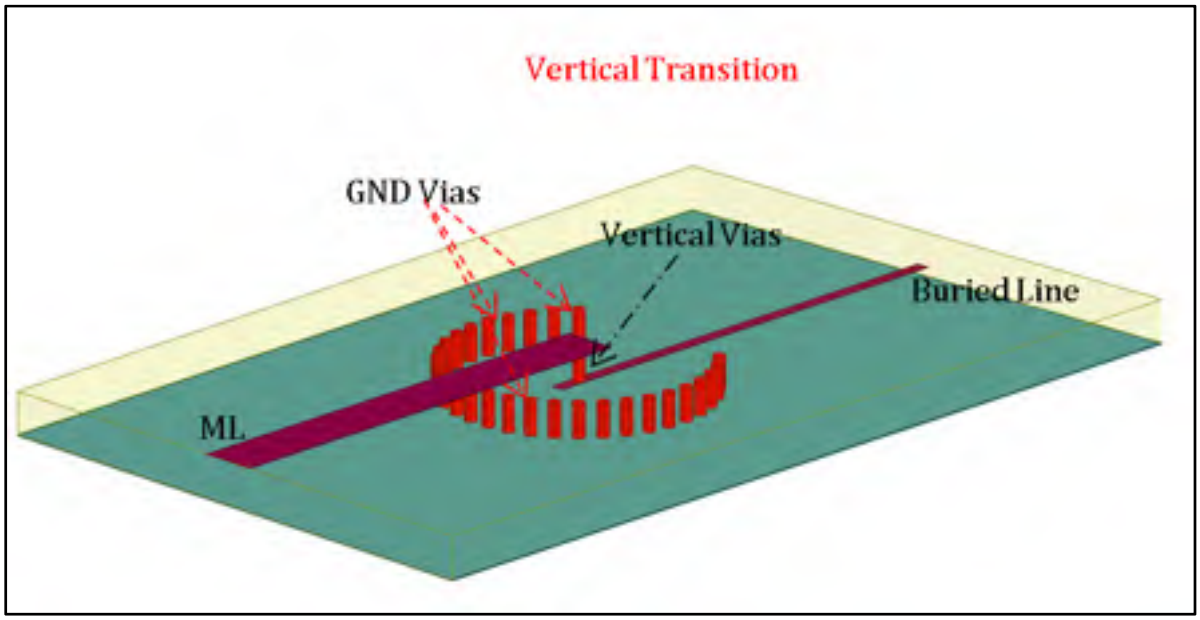

Figure 3.6Perpendicular transition models in HFSS

The proposed vertical transition structure uses Ferro L8 substrate that has dielectric constant of 7.2 has the thickness of 635 um. All the grounded vias are connected to the ground plane which is located at the bottom of the last layer of the substrate. The width of the microstripline is W1= 853 um and that of the buried line is W2= 127 um as well as the height from the buried line to the grounded via was equal to 127 um as seen in Figure 3.1, The height of all vias is 508 um and the distance between the center via and the grounded (veil) vias is 1000 um. These dimensions have been optimized in order to obtain a coaxial line where the signal transmits according to TEM mode between the inner and outer connector. Figures 3.7 and 3.8 present the side and top views, respectively, of the proposed transition.

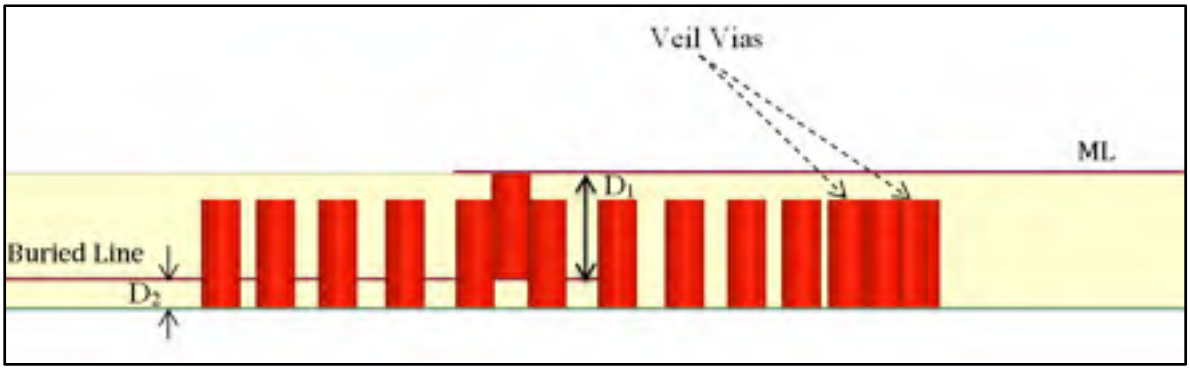

Figure 3.7Side view of vertical transition. D1=508 um and D2=127 um

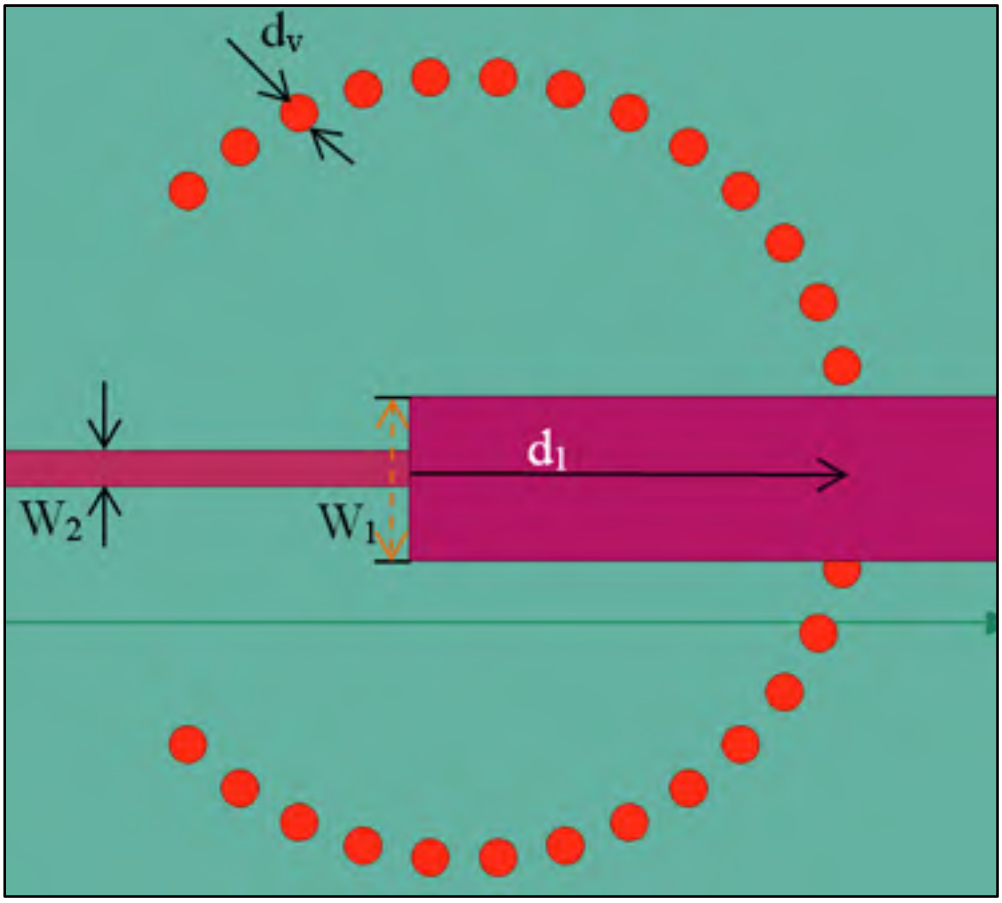

Figure 3.8Top view of the vertical transition with W1=853 um, W2=127 um, dv =150um,D1=1000 um

3.4 3D Four-Port Reflectometer: Version 1

By combining the micostripline,the sniffers and the vertical transition, a new 3D 4-port reflectometer can be created with small size, low-cost, and ease of integration for embedded vector (amplitude and phase) measurement with good measurement accuracy and with no interfering between the sniffers and other transmission lines. Further, because of the simple structure of the sniffers, we can place them at any distance that is less than $\lambda/4$. So, we are able to design different structures of reflectometers with different spacing between the sniffersin order to obtain a vector measurement for different frequencies and applications. Figure 3.9a,b,c, d present the final design of the proposed reflectometer with different spacing (d) expressed in wavelength. For the four designs shown, the spacing between the sniffers sit at $\lambda/11$,$\lambda/20$,$\lambda/25$, $\lambda/40$.

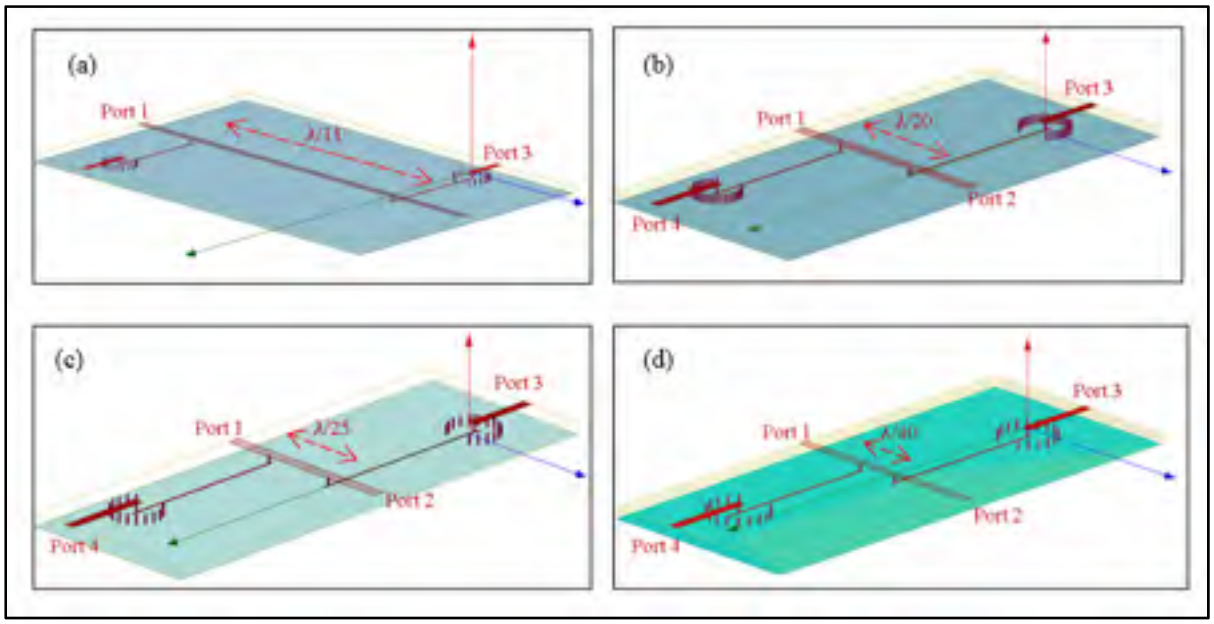

Figure 3.9 a, b, c, dDifferent 4-port reflectometers prototypes at varying sniffer spacing

3.4.1 EM Simulation

The ANSYS HFSS is a 3D electromagnetic (EM) simulation for designing and simulating high- frequency electronic products such as antennas, antenna arrays. This simulator is used to compute the S-parameters of the proposed complete 3D reflectometer shown in Figure 3.9.

Our focus is onobtaining good matching at all ports with less than -20 dB reflection coefficient for S_{11} and S_{22}, a low coupling less than – 30 dB for S_{31} and S_{41}. The simulation results show that S_{11} and S_{22} for all structures are below -20 dB and that the insertion loss, S_{21}, is -0.1 dB as seen in Figure 3.1a,Similarly, S_{31} and S_{41}in Figure 3.10b show low coupling around -30 dB, which is the coupling that we are expected to get at the coupling ports of the proposed reflectometer to measure the output coupled power.

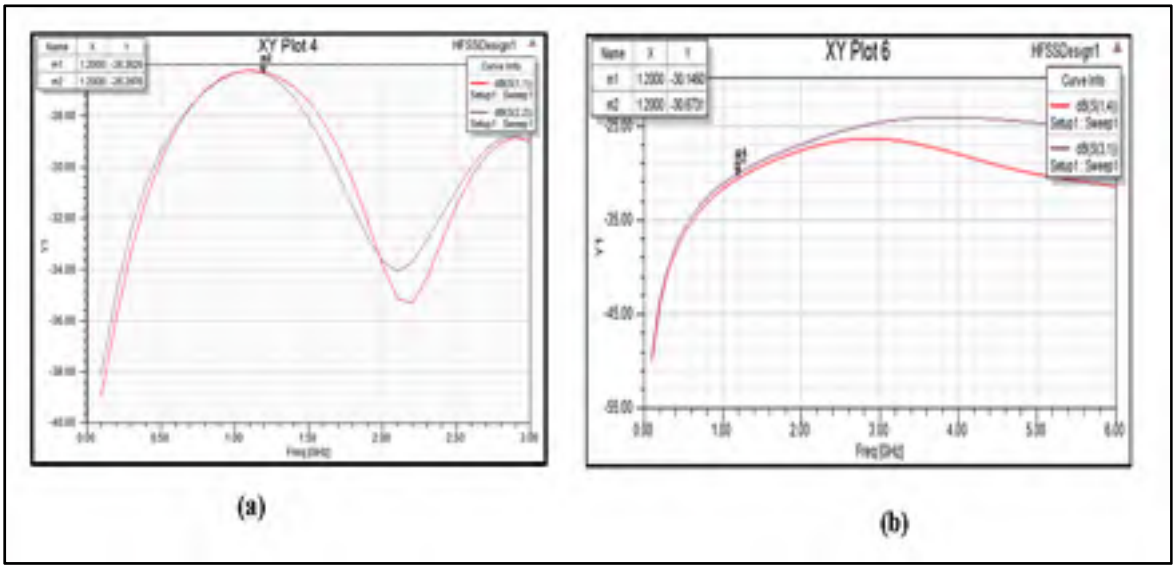

Figure 3.10(a) simulated S11 and S22 in dB, (b) simulated S31 and S41 in dB

3.4.2 Fabrication in LTCC Technology

The proposed reflectometer has been fabricated on low temperature co-fired ceramics (LTCC) substrate, which has advantages of low cost, high performance and the availability of a wide range of materials, such as Ferro A6 and Ferro L8. To fabricate our designed structure, Ferro L8 material is used. We usedthree layers of 10 mils thick sheets and one 5

mil-thick sheet in the stack. We also used silver paste to fill the vias and to print the microstrip and buried lines.

The fabrication process proceeded as follows. First, the process is started with via punching on each single sheet, then via filling by the silver paste followed by printing the lines on the proper sheets. The next step was stacking all the sheets together to get a single stack. Because we included different designs on one 10 cm x 10 cm stack, cutting was the necessary next step to separate the designs into individual pieces. After that, the last step consisted of co-firing the cut pieces into the oven between 4 to 6 hours following a specified temperature profile with a maximum of$875^0\ C$. Figure 3.11 shows different fabricated prototypes of the final proposed 3D four-port reflectometer configurations.

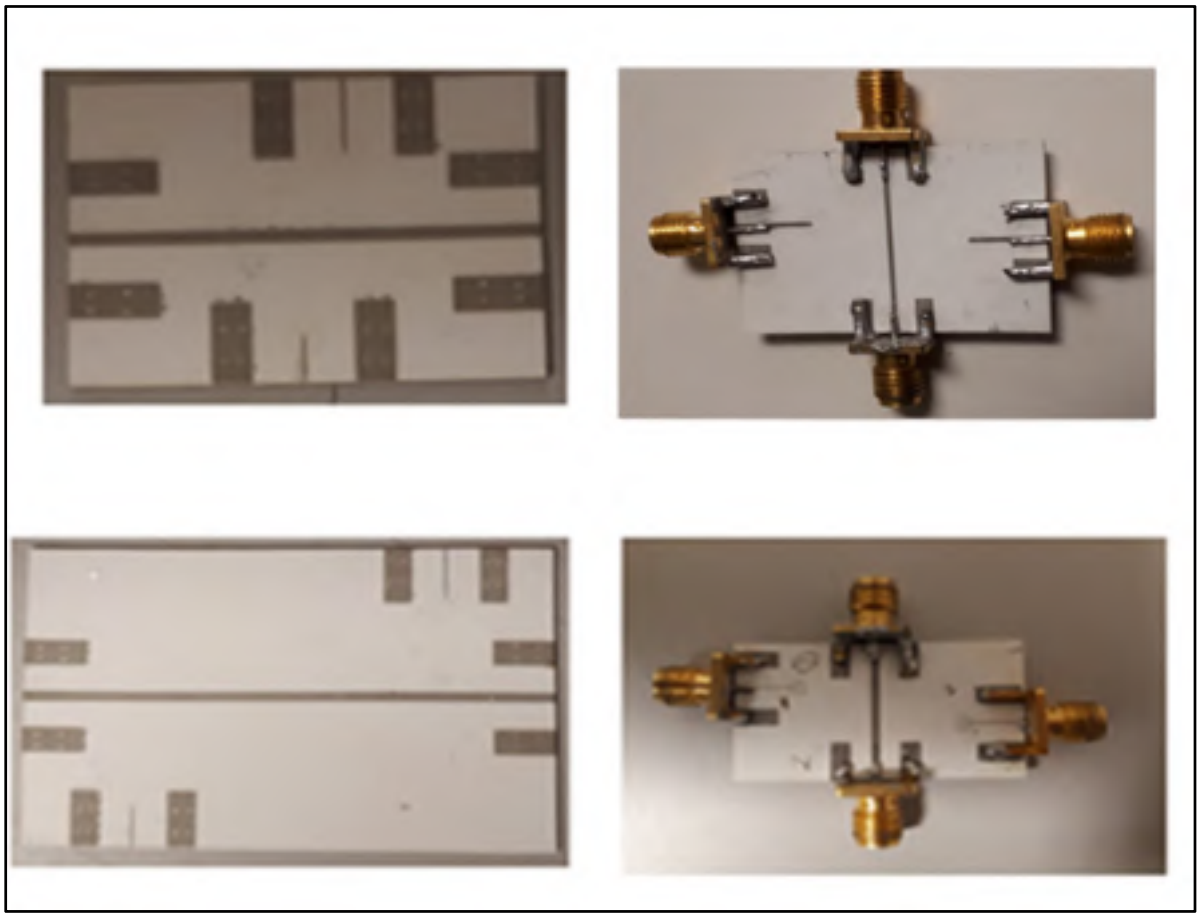

Figure 3.11Fabricated prototypes of the different 4-port reflectometer configurations

3.4.3 S-Parameters Measurement of the 3D 4-port Reflectometer

In order to measure the parameters of a multi-port network, waves must be inserted at the a selected port while each of the other portsisterminated by a matched load equal to system'sreference impedance Zo (usually 50 Ω). For a two-port network, the explicit definitions and measurement conditions of the S-parameters are as follows:

$$S_{11} = \frac{b1}{a1} whena2 = 0 = \frac{V_1^-}{V_1^+} Reflectioncoefficientatport\ 1 \tag{3.4}$$

$$S_{21} = \frac{b2}{a1} whena2 = 0 = \frac{V_2^-}{V_1^+} Transferratioport\ 1\ toport\ 2 \tag{3.5}$$

$$S_{12} = \frac{b1}{a2} whena1 = 0 = \frac{V_1^-}{V_{12}^+} Transferratioport\ 2\ toport\ 1 \tag{3.6}$$

$$S_{22} = \frac{b2}{a2} whena1 = 0 = \frac{V_2^-}{V_{12}^+} Reflectioncoefficientatport\ 2 \tag{3.7}$$

It is worth noting that every parameter is a complex quantity. So, for instance, the angle indicates phase difference in degrees, whereas the magnitude indicates the ratio between the amplitudes in dB (David M. Pozar, 1998).

$$S_{ij} = |S_{ij}|e^{j\theta} \tag{3.8}$$

$$S_{ij}(dB) = 20\log_{10}|S_{ij}| \tag{3.9}$$

The fundamental of vector network analyzers (VNAs) has been covered in chapter 2 as one of the techniques that measures the amplitude and phase of signal ratios. The use of a VNA requires a calibration prior to measuring devices. A full two-port calibration procedure is used to calibrate the Agilent HP8753ES VNA used to measure our reflectometer prototypes. This calibration is based on the SOLT (Short-Open-Load-Through) technique which achievescorrection for cable length and loss and all internal instrument impairments. The

calibration standards used are those of the 85052D 3.5 mm calibration kit. Calibration was carried out between 1 and 1.4 GHz with the center frequency being our design frequency, namely 1.2 GHz.

The S-parameters of the fabricated prototype were obtained using the vector network analyzer VNA(Agilent HP8753ES) with the input power range of -5 t0 -10 dBm over the frequency range of 1 GHz to 1.4 GHz. Since this VNA has only two ports, multiple connections and measurements were carried out sequentially by connecting the VNA to two of the ports and terminating the others with 50 Ω termination loads as shown in Figure 3.12.

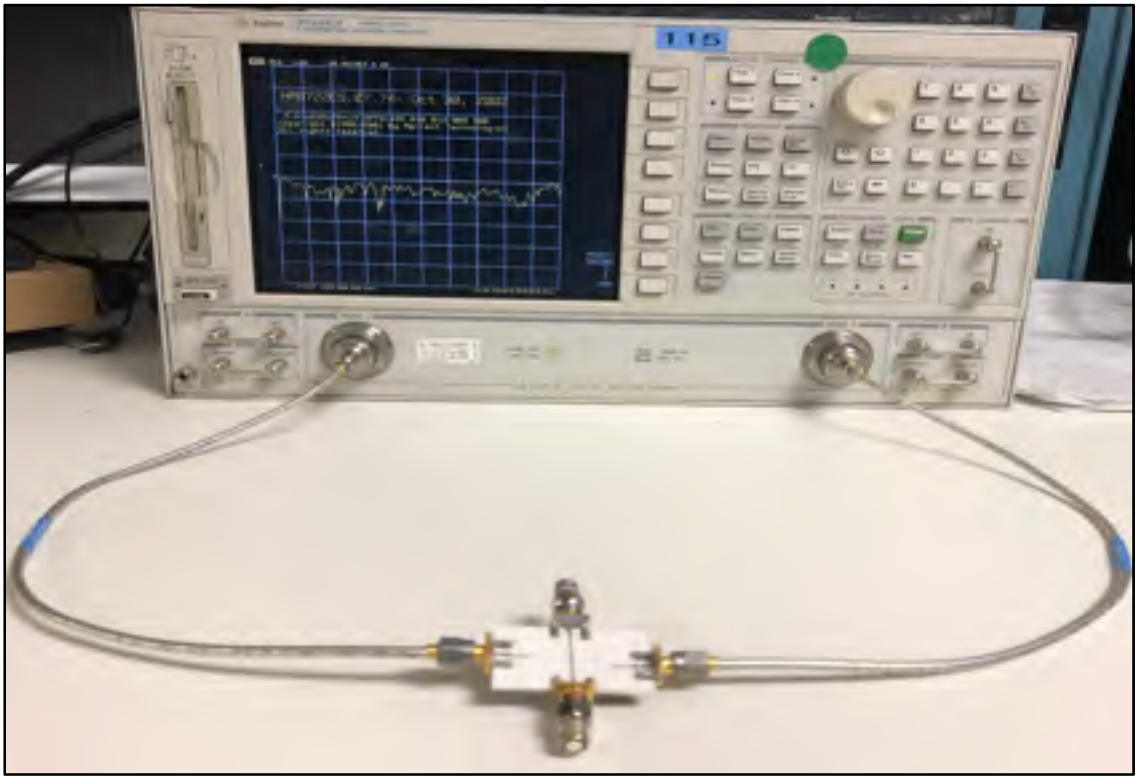

Figure 3.12S-parameters measurementsetup of the fabricatedreflectometer prototype using a commercial VNA

The measured S-parametersof the proposed prototype are presented in Figure 3.13 The measured return losses RL of the prototype are marked around -15 dB which is higher than the simulation results. However, the measured coupling at ports 3 and 4 are around -30 dB as

predicted in simulation. The lack of good RL levels will have an impact on the precision of the measurements using the reflectometer and will be further addressed in section 3.5 where a second improved version of the reflectometer is proposed.

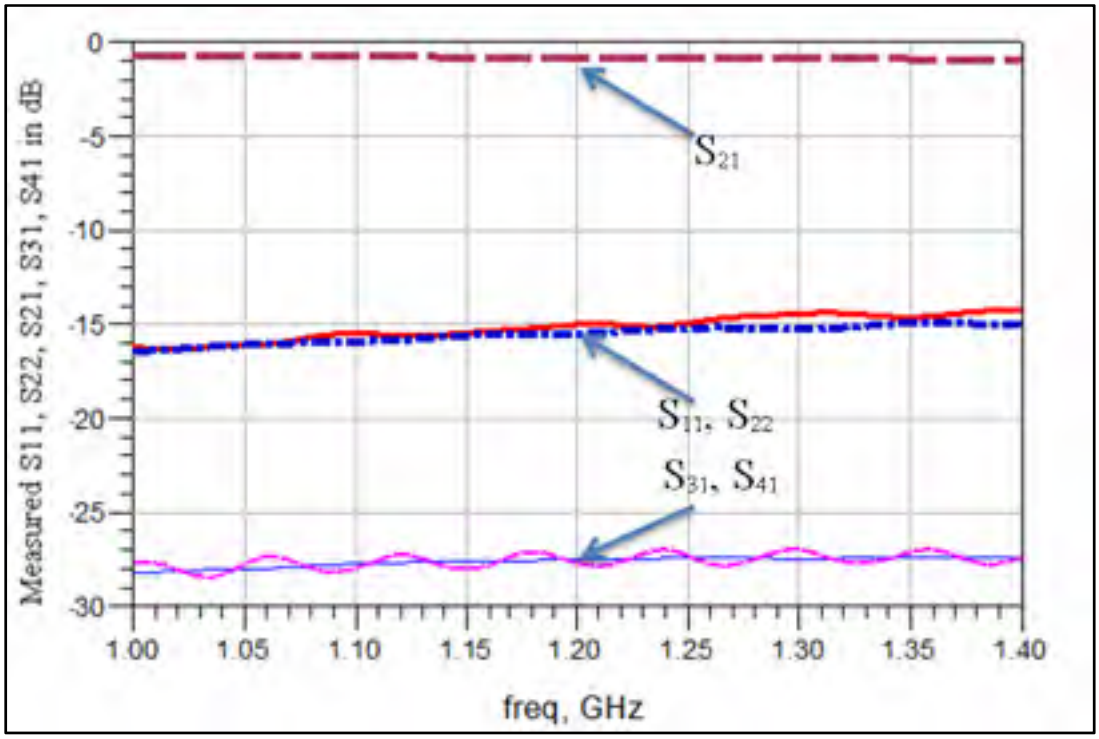

Figure 3.13Measured S-parameters of the 4-port reflectometer

3.4.4 Coupled PowerMeasurement using Power Meter

The power meter is an instrument that is used to measure an RF signal's power with high precision and over wide frequency ranges and power levels. In the previous work (A. B. Kouki, et al., 2010), power meters were used to measure the output power at port 3 and 4, namely P3 and P4, which are then used in equations 2.11 and 2.12 to determine the complex reflection coefficient. Here, we propose to also use power meters as first step and more easily integrable power detectors at a second step. To this end, an external Agilent E4417A power meter is connected to port 3 and 4. Next, a 0 dBm power input signal is injected at port 1 while several different loads (DUTs) are connected at port 2 and the power meter readings at ports 3 and 4 are noted. This is repeated for three different frequencies, namely 1, 1.2, and

1.4 GHz. Table 3.2 summarizes the obtained measurements when DUT is a 50 Ω matched load.

Table 3.2 Coupled power measurement using theE4417A power meter with 0 dBm input power and 50 Ω termination different frequencies.

Loads	Frequency	Input power	P3dBm	P4dBm
50 Ohm	1 GHz	0 dBm	-27.989	-27.643
50 Ohm	1.2 GHz	0 dBm	-27.513	-27.556
50 Ohm	1.4 GHz	0 dBm	-27.413	-27.388

3.4.5 Coupled PowerMeasurement using the LT5582 Power Detector Circuit

The need for the integration to achieve small size and low cost embedded RF measurements means that power meters are not an option for power measurement. Indeed, the power meter is still an external instrument that cannot be integrated for embedded measurement. Therefore, we consider the alternative of using a power detector chip instead. The LT5582 RMS power detector, from Analog Devices, is capable for measuring the RMS power and has been used for several applications such as PA power control and receiving and transmitting gain control. Also, it has the features of the small size of the circuit which is 3 mmx3 mm and a dynamic range of 57 dB. It also shows low linearity error over its entire dynamic range and covers a wide frequency range from 40 MHz up to 10 GHz. Figure 3.14a presents the circuit schematic from the data sheet with the LTC5582 IC and different resistors and capacitors at the input and the output of the circuit. This detector requires a 3.3V supply voltage, a 3.3V enable voltage, and can has a maximum input power of 18dBm. It is rated to operate between-40^0 C to 85^0 C. A prototype of this detector was designed, following the company's reference design, and fabricated on a Rogers's substrate with dielectric constant 6.15 as shown Figure 3.14b. This design can be easily be implemented in LTCC as a step to reach the full circuit integration with the proposed reflectometer.

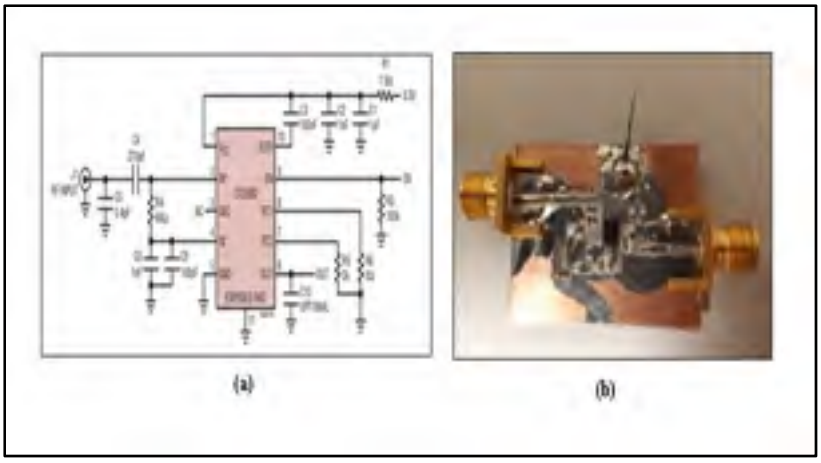

Figure 3.14(a) Shows the LTC5582 circuit from the datasheet(b) LTC5582 fabricated circuit on Roger Substrate

In order to examine and test the fabricated circuit, we first characterize the detector response. To do this, the input of the circuit is connected to a signal generator which injects different input power levels while the output port is connected to an oscilloscope which reads the output voltage. This test setup is presented in Figure 3.15. The graph in Figure 3.10ashows the output voltage response versus the input power from the data sheet with linear response of the input power until -57 dBm for several frequencies between 450 MHz and 5.8 GHz. The graph in Figure 3.10b presented the measured response of the fabricated prototype for a similar power range at 1.2 GHz. The obtained result is quasi-linear which confirms that the fabricated circuit can operate close to the manufacturer's specifications.

With the basic detector circuit characterized and validated, next we produce two detector circuits and connect them to the coupling ports 3 and 4 of the reflectometer. Again, we apply a 0 dBm RF signal at input port (port 1) and place a 50 Ω termination load at the output port (Port 2). Table 3.3is sumurizes thecoupling measurement using the LTC5582 power detector circuits with 0 dBm input power at different frequencies. These results are similar to those obtained using power meter measurements. It is therefore possible to use the LTC5582 power detector circuits at different frequencies without loss of accuracy in measurements.

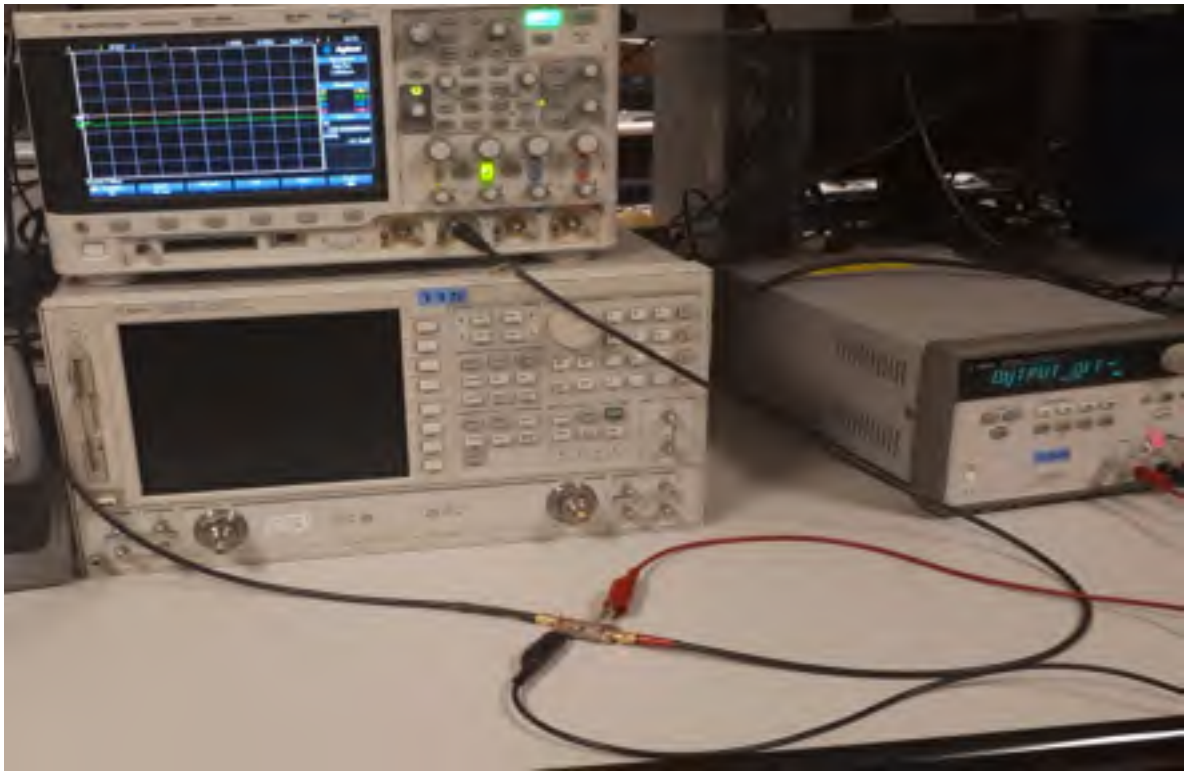

Figure 3.15Test setup to characterize the fabricated LTC5582 power detector

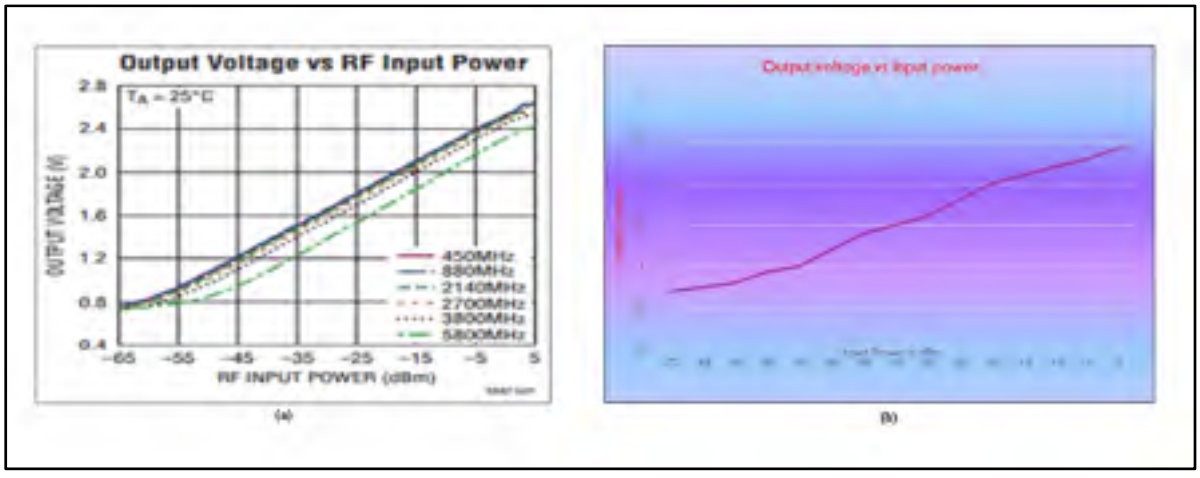

Figure 3.16(a)Output Voltage vs RF Input Power (data sheet),
(b) The measured output voltage vs input power for
the fabricated LTC5582

Table 3.3Coupling measurement using LTC5582 power
Detector circuits with o dB input power at different frequencies

Loads	Frequency	Input power	P3dBm	P4dBm
50 Ohm	1 GHz	0 dBm	-27.987	-27.621
50 Ohm	1.2 GHz	0 dBm	-27.523	-27.546
50 Ohm	1.4 GHz	0 dBm	-27.410	-27.375

3.4.6 Reflection Coefficient Measurement

At this stage, we are reaching at the last step of our research problem which is the validation of the theory in chapter 2 and the feasibility of the proposed 3D reflectometer as an embedded measurement circuit. To do this, we need to measure reflection coefficients of different loads using both the commercial VNA and our 3D reflectometer with the LTC5582 power detectors. To generate different load impedances, we use a double stub tuner with one port terminated by a 50 Ω load and other port connected to the VNA, as shown in Figure 3.17. We start with the VNA measurements at 1.2 GHz for a set of different loads corresponding to different double stub settings. In all 45 different loads are generated and measured.

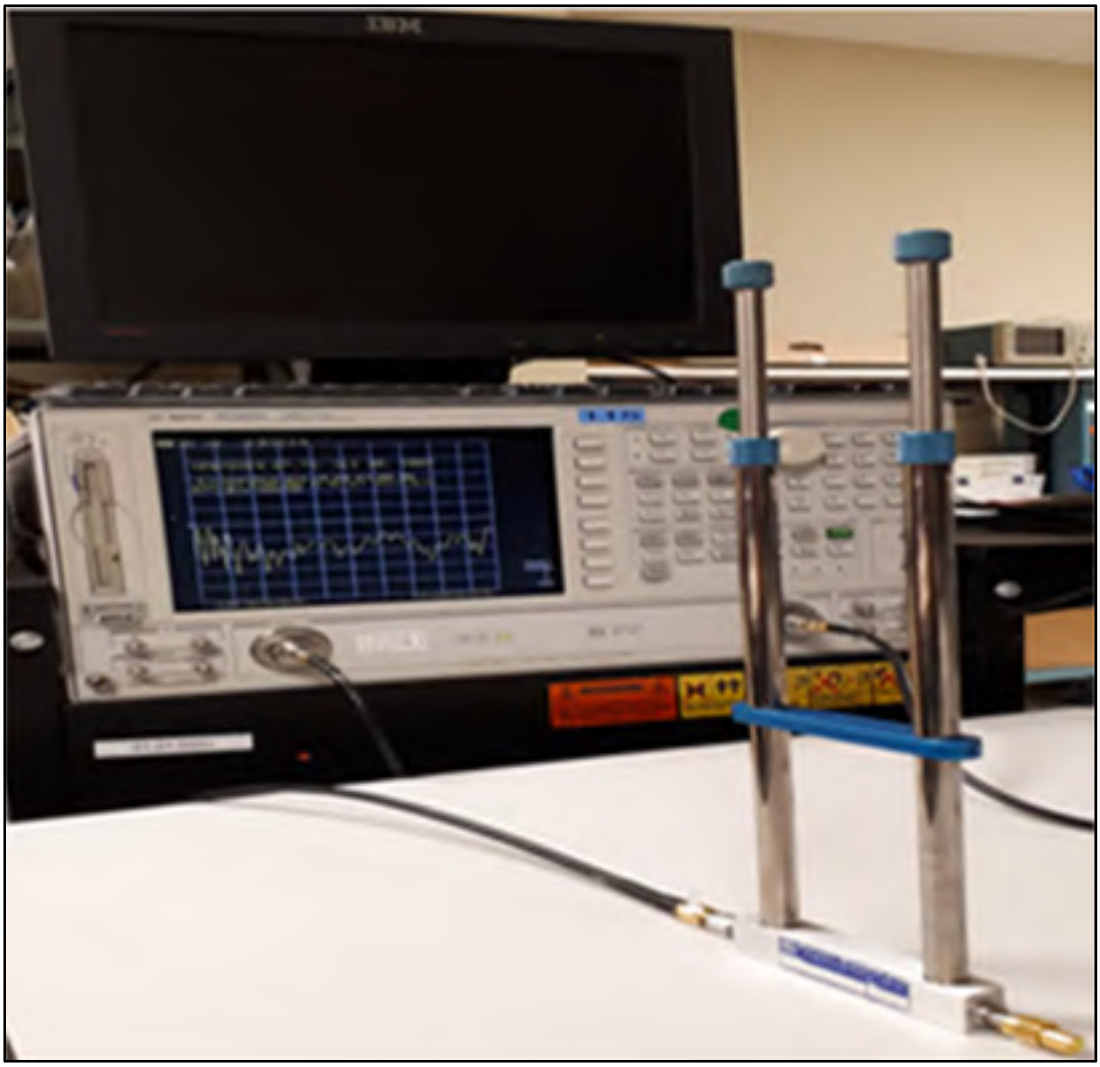

Figure 3.17Test setup for reflection coefficient measurement using a VNA

Second, we perform similar measurements using the proposed reflectometer with 0 dBm RF input power injected in port 1, while the manual double stub tuner is connected to port 2 as shown in Figure 3.18. The same double stub tuner settings for the 45 loads used with the VNA are repeated for the reflectometer.

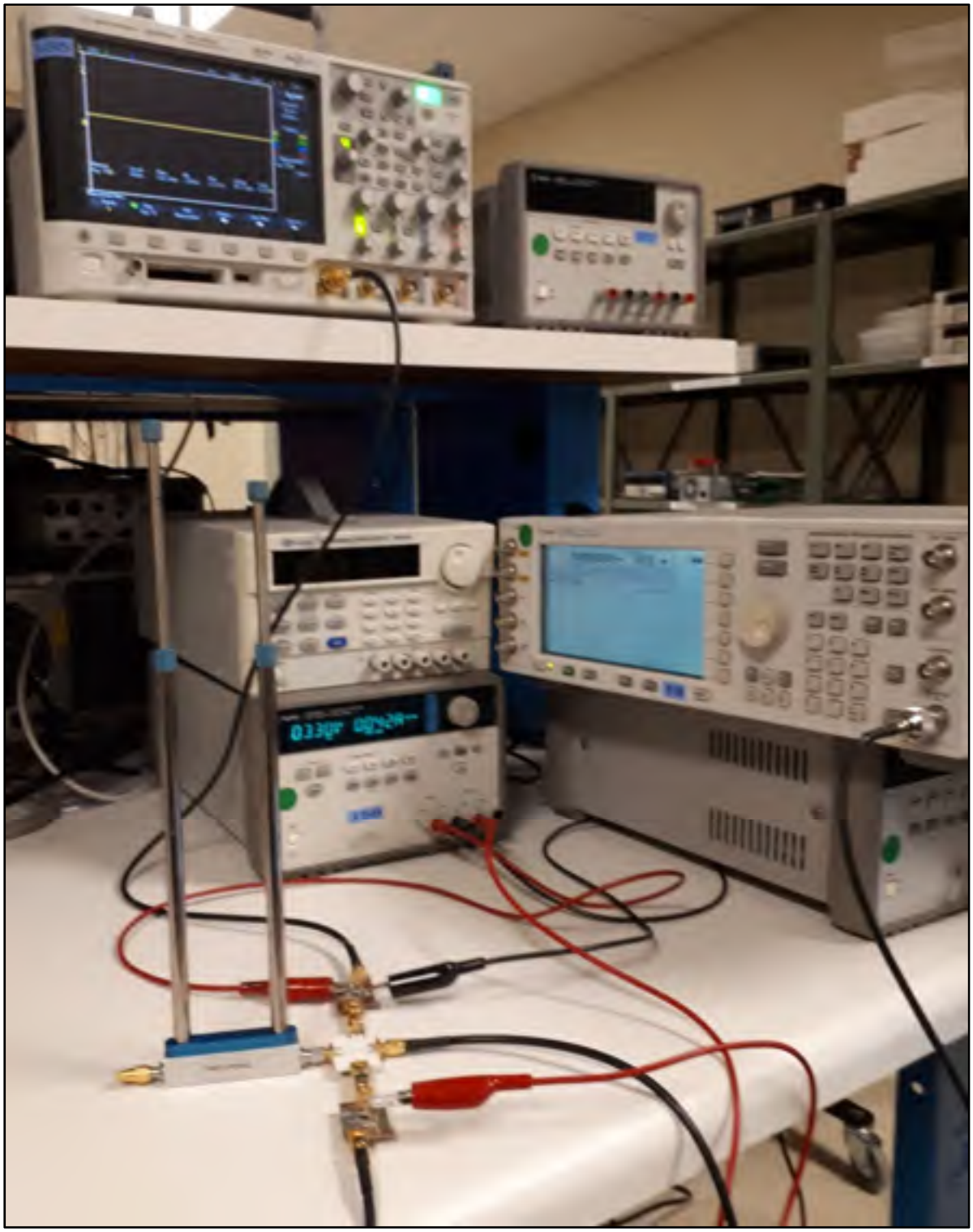

Figure 3.18Test setup for reflection coefficient measurementwith the reflectometer

For each load, the stored S-parameters of the proposed reflectometer, obtained in 3.3, and the two measured powers (P3 and P4) with the LTC5582 are used to draw the intersection of two circles of equations 2.11 and 2.12 in Matlab (see APPENDIX II). The intersection point determines the precise complex reflection coefficient for the given load as shown in Figure 3.19.

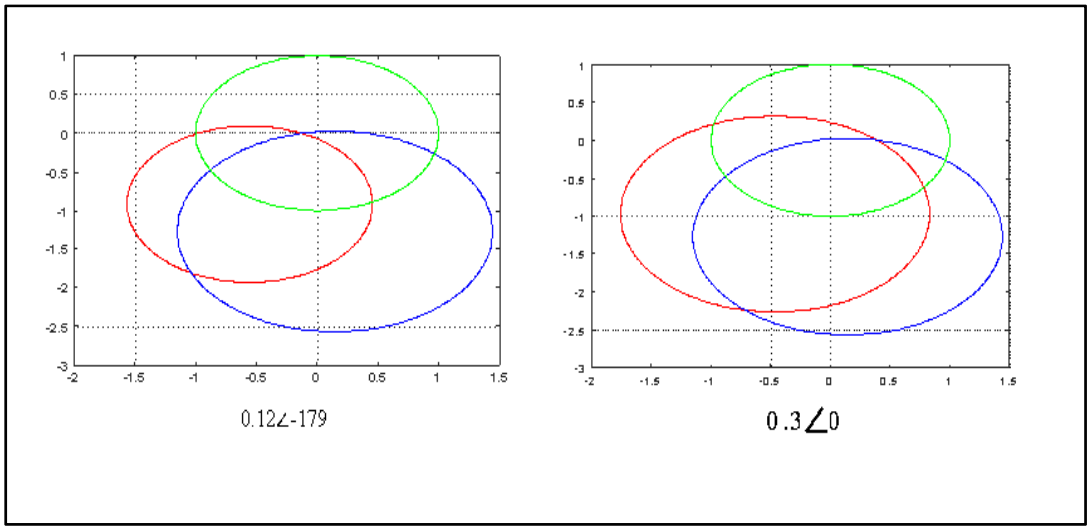

Figure 3.19Intersections of two circles using Matlab todetermine
the precise complex reflection coefficient
(the unit circle is in green)

Figure 3.20 presents the reflection coefficient measurements of 45 different loads using the VNA and the proposed 4-port reflectometer. This figure also shows the error in magnitude, in dB, and in phase, in degrees, between the VNA and reflectometer measurements.

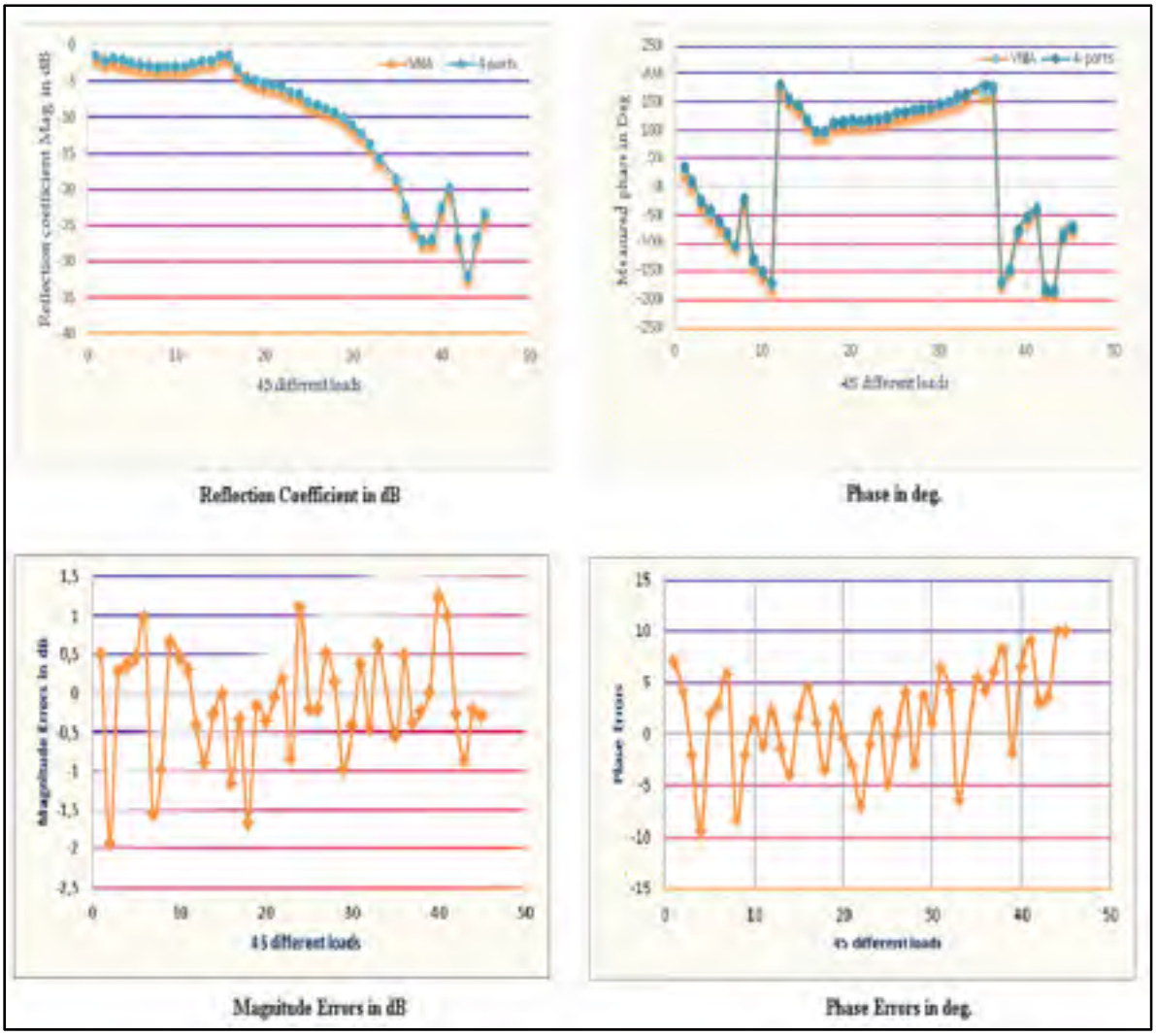
Reflection coefficient Mag. in dB
45 different loads
VNA
4 ports
Reflection Coefficient in dB
Measured phase in Deg
45 different loads
Phase in deg.
Magnitude Errors in dB
45 different loads
Magnitude Errors in dB
Phase Errors
45 different loads
Phase Errors in deg.

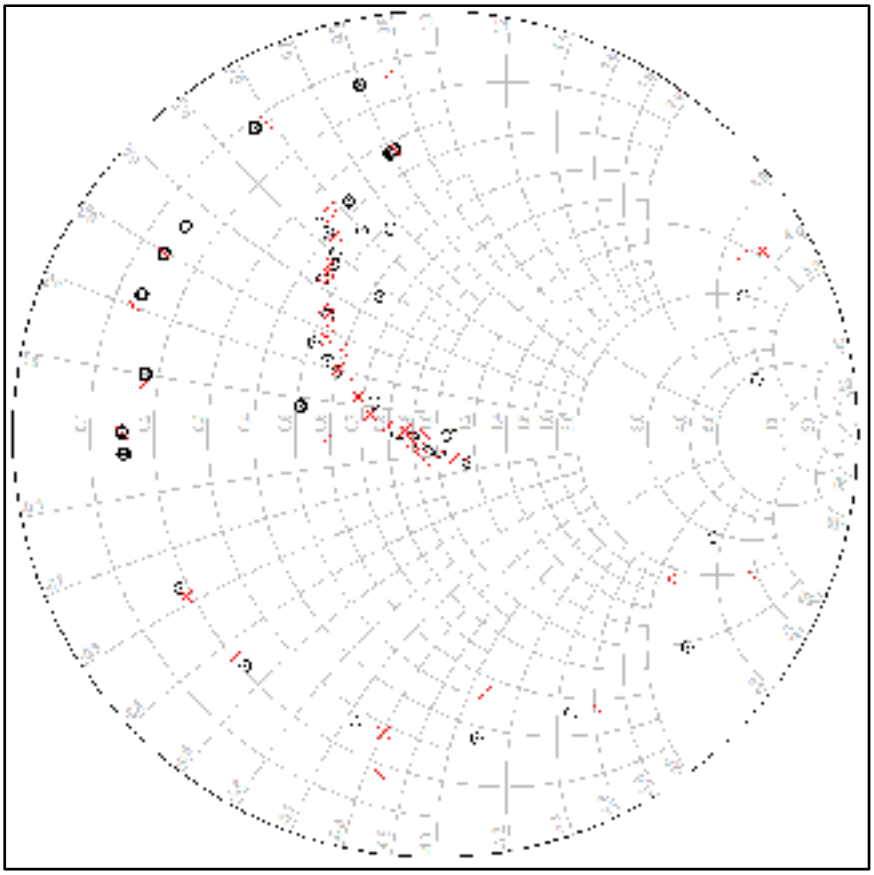

Figure 3.20 Measured magnitude and phase of the reflection coefficientfor45 different loads and errors in magnitude and phase between the VNA and reflectometer measurements with smith chart plotting

3.4.7 Discussion of Results

Based on Figure 3.14, the proposed reflectometer gives a maximum error in magnitude around 2 dB and a maximum error in phase of around 10^0. While such precision may be sufficient for many applications, we propose to investigate ways of improving the accuracy of our proposed reflectometer. As stated previously, the lack of good RL level at ports 3 and 4, which is due to the vertical transition on the sniffer lines not being optimal, is expected to be the main cause for the accuracy performance obtained. Therefore, we propose to optimize the vertical transition further in a second prototype of the reflectometer.

3.5 Version 2: Prototype 3D Four-port Reflectometer

In version 1, the proposed reflectometer included a vertical transition made of a central via surrounded by ground vias to approximate a coaxial line. The measured S-parameters of the fabricated prototype were different from simulation and displayed an insufficient level of matching. This lack of performance is mainly due to the vertical transition. Therefore, we propose a new version of this transition where we focus on improving its S-parameters by achieving good matching at all ports. The vertical transition will therefore be further optimized through the use of more standard and non-standard vias. Once this is achieved, a similar methodology to what was done with version 1 will be followed for simulation, fabrication, and measurement.

3.5.1 Optimization of the Vertical Transition

To improve the transition, two main modifications were introduced and simulated. The first, consisted of using solid vias, i.e., the vias surrounding the center via are replaced by a single solid arc Figure 3.21 a. The second consisted of extending the vias alongside the buried line as shown in Figure 3.21. A third variation consisted of replacing all standard circular vias with solid rectangular vias as shown in Figure 3.21. The filled solid arc via has a radius (dr) of 420 um and the width (Wr) of 225 um.

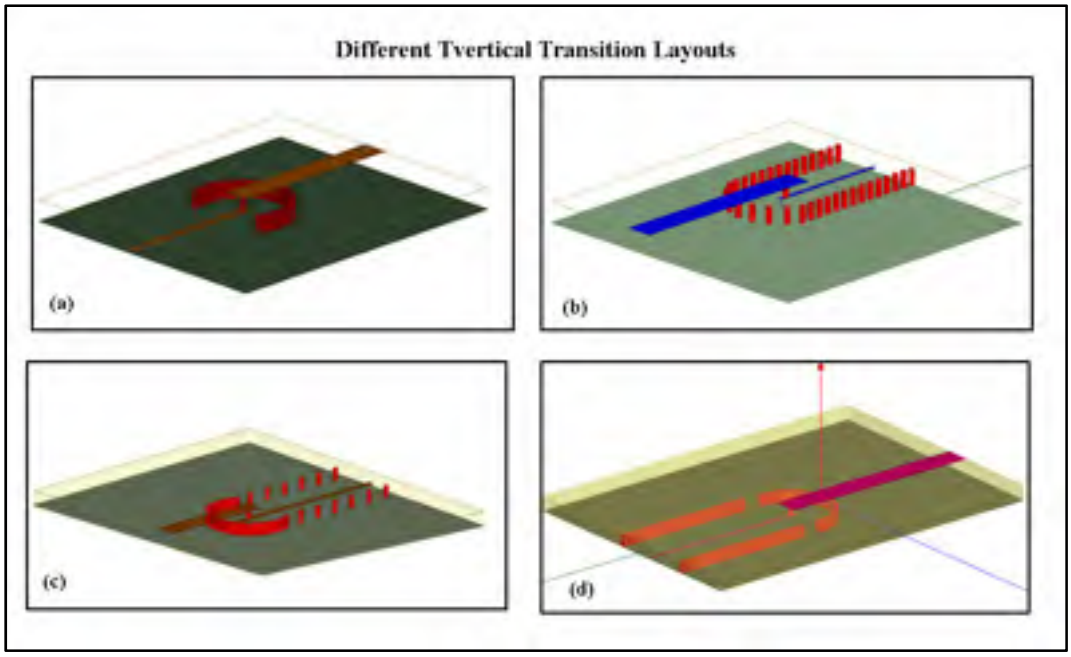

Figure 3.21a) arc line with grounded lines b) circles of vias with grounded vias along the buried line c) Top view of the arc via and side view d) the side and top view of the circled vias

3.5.1.1 Simulation and Measurement Result

In order to simulate and measure the new proposed transition design, a back-to-back transition configuration was used as shown in Figure 3.22 using both rectangular and circular vias. Our target performance is a return loss less than -20 dB at both ports. Figure 3.23a shows the results of the HFSS simulation for the transition with rectangular vias while Figure 3.23b gives the results for the transition with circular vias. As can be seen from these results, the return loss at both ports is below -25 dB over the entire frequency band from 100 MHz to 3.5 GHz. Both transitions were fabricated side by side as shown in Figure 3.24.

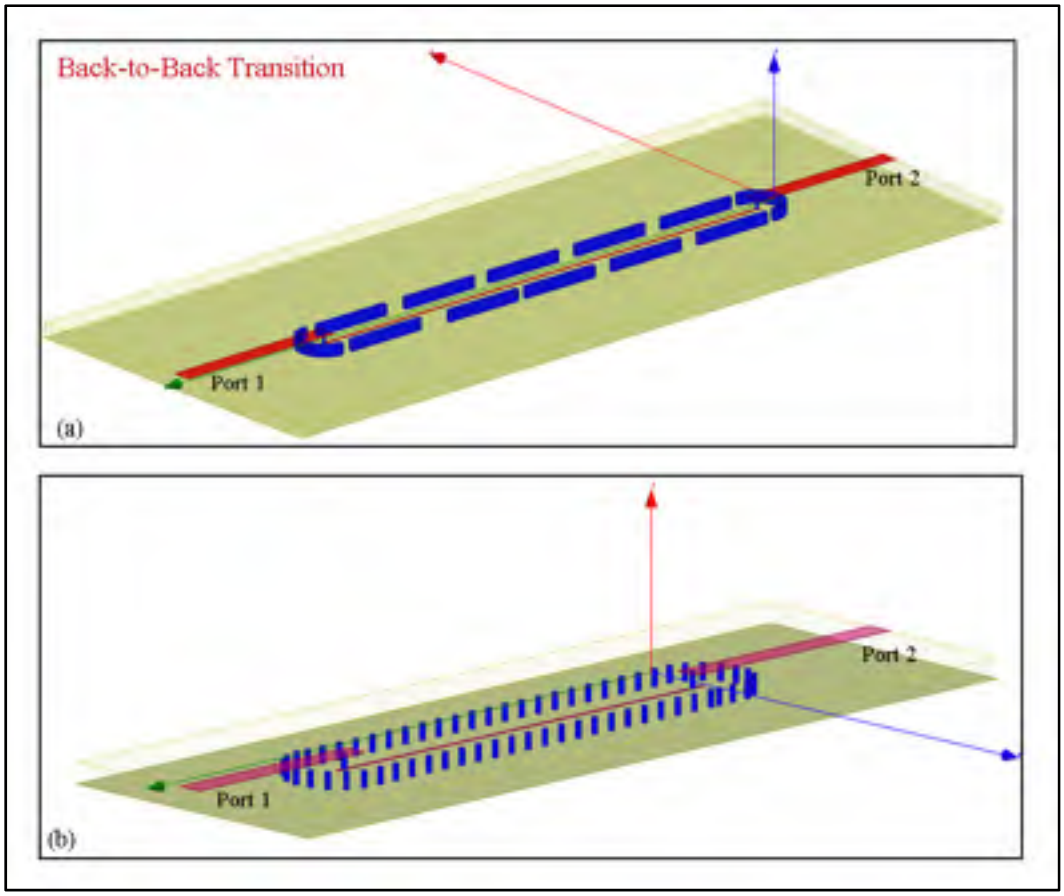

Figure 3.22a) Back to back transition surrounded with rectangular vias
b) Back to back transition surrounded with circular vias

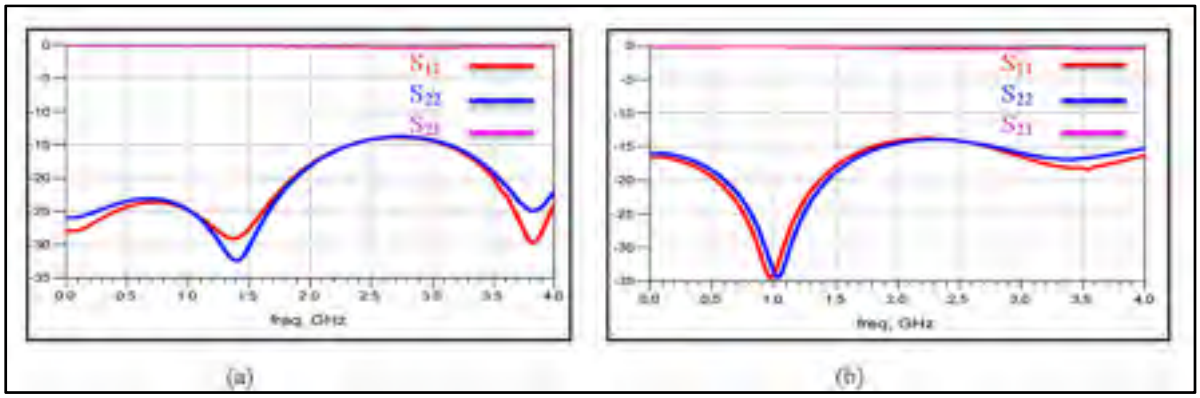

Figure 3.23Simulation result of vertical transitionsurrounded
witha) rectangular viad, b) circular vias

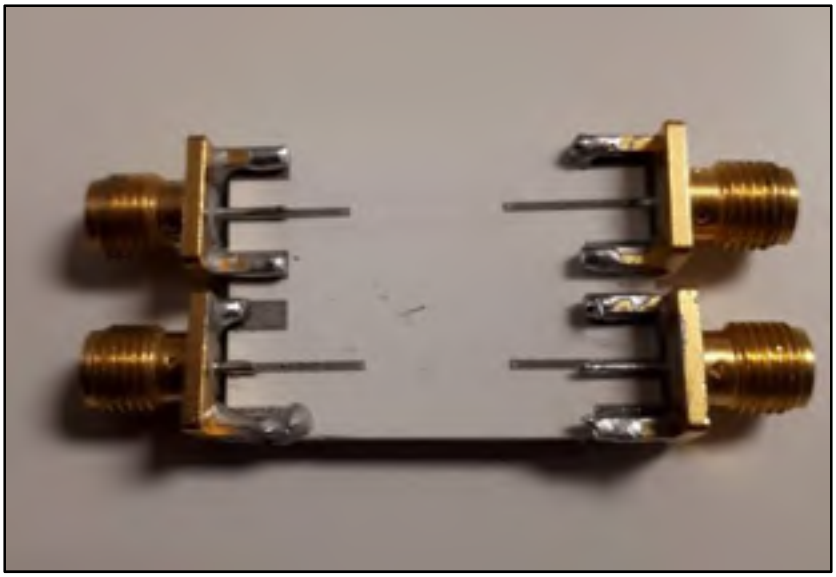

Figure 3.24Fabricated optimized transition prototype

To measure the S-parameters of the new transition design, the same measurement setup described in 3.4.3 is used. Figure 3.25 presents the measured S-parameters and shows that S_{11} and S_{22} are better than -18 dB up to 2.8 GHz. The insertion loss does not exceed -0.932 dB.

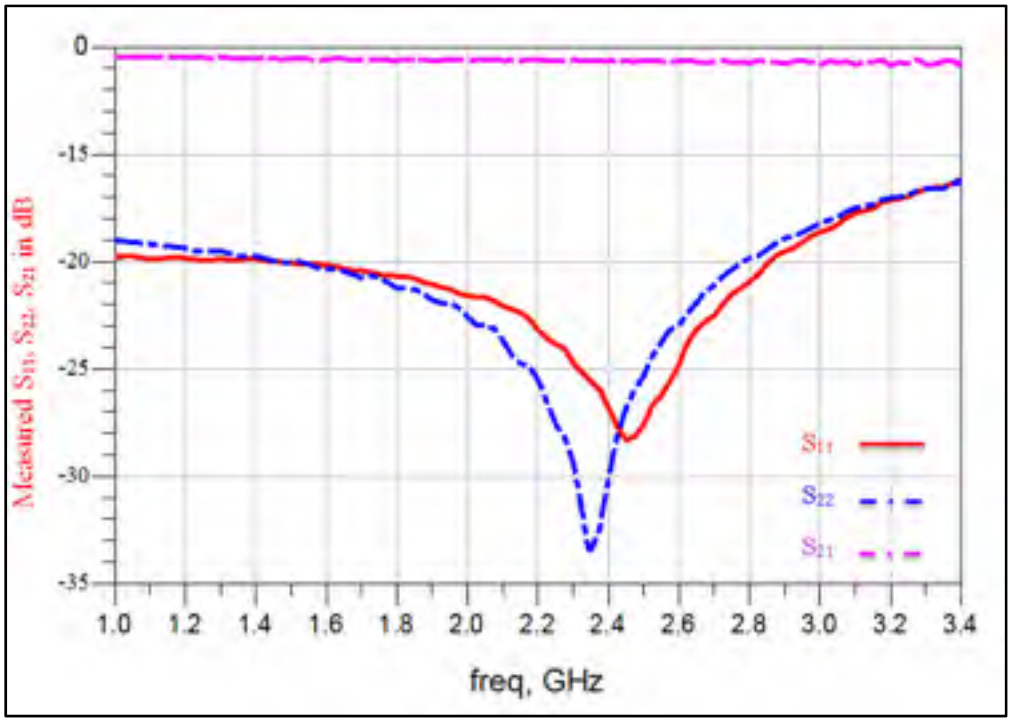

Figure 3.25 Measured s-parameters of the optimized transition

3.5.2 The Effect of Adding Grounded Vias on the Performance of the 3D 4-port Reflectometer

Given the improvement achieved with the addition of vias in the previous section, in this section we apply grounded vias gradually to the full reflectometer structure. We choose a sniffer spacing of $\lambda/_{40}$and compare different structures as shown in Figure 3.26. Figure 3.26(a) shows the four-port reflectometer with the solid arc rectangular via only while Figures 3.25 (b)-(d) show the same structure with grounded circular vias added gradually.

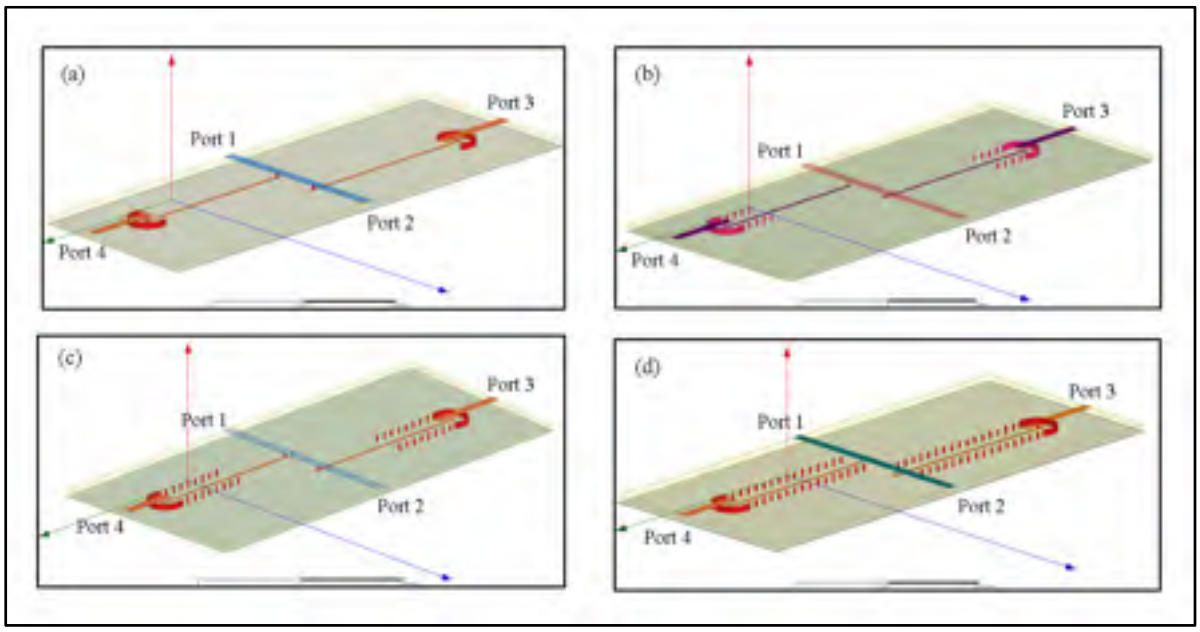

Figure 3.26a) Four-port reflectometer with arc solid line around the center vais b, c, d) four- port reflectometer with arc solid line around the center vais with gradual grounded vais added to each prototype

Figure 3.27 (a, b, c, and d) present the simulated S-parameters for each the four structures of Figure 3.26. As can be seen from these simulation results, the more vias are added the better the matching is obtained. Next, the four structures were fabricated and measured between .5 and 6 GHz. The measurement results are shown in Figure 3.28. While the measured results do not follow the simulation of the entire band, nonetheless, they are better than those of the first reflectometer prototype and show excellent performance at 1.2 GHz, our frequency of interest.

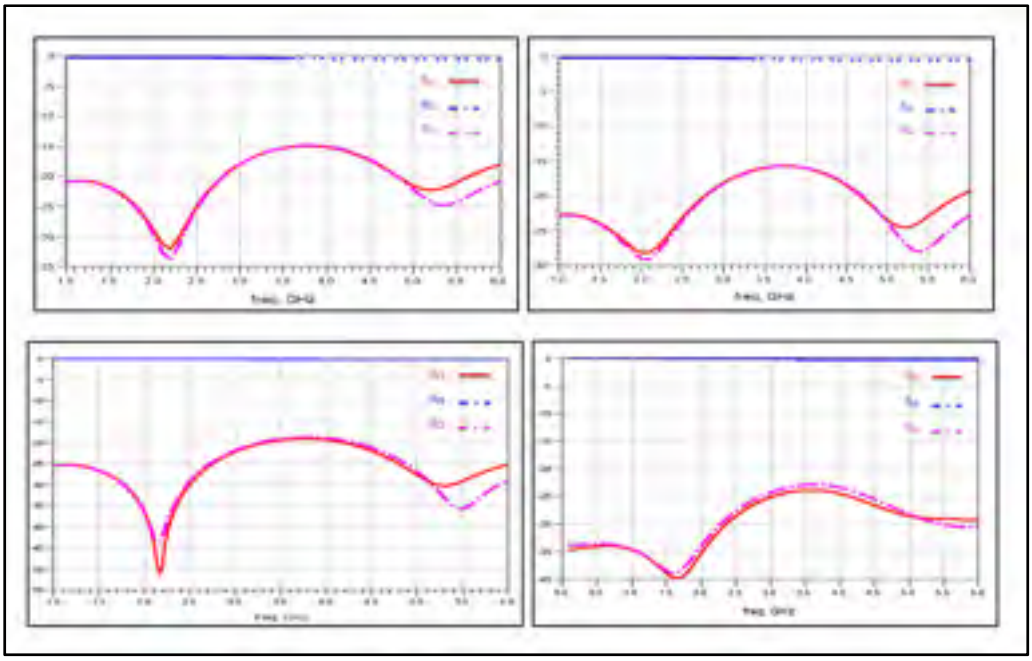

Figure 3.27Simulated S-parameters of 3D 4-port reflectometer with differentoptimized layouts

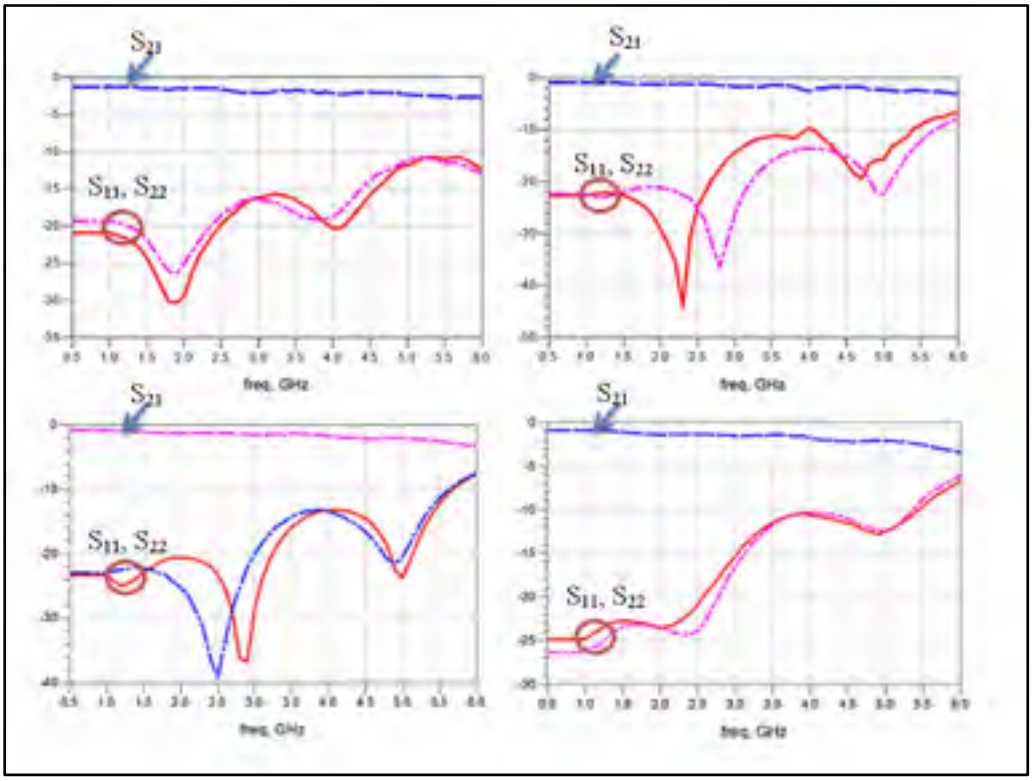

Figure 3.28Measured S-parameters of 3D 4-port reflectometer for different sniffers optimizations

3.5.3 Reflection Coefficient Measurements using power Detector Circuits and Equation written on Matlab Code for Optimized Prototype

Based on the results of the previous section, the fabricated prototype of Figure 3.29 is chosen, as it gives the best performance, to perform reflection coefficient measurements of varying loads. Here we repeat the measurements that were carried out with the first reflectometer prototype for the same 45 loads. We again compare the obtained results of the reflectometer measurements to those of the VNA in Figures 3.30 (a) and (b), for magnitude and phase, respectively. Figures 3.30 (c) and (d) present the error in magnitude and phase between the reflectometer and VNA measurements. As can been seen, the maximum magnitude error is around 0.3 dB, down from about 2 dB for the first prototype, and the maximum phase error is around 3^{o}, down from 10^{o} for the first prototype. Figure 3.31 presents the measurement results of the reflection coefficient plotted on smith chart.

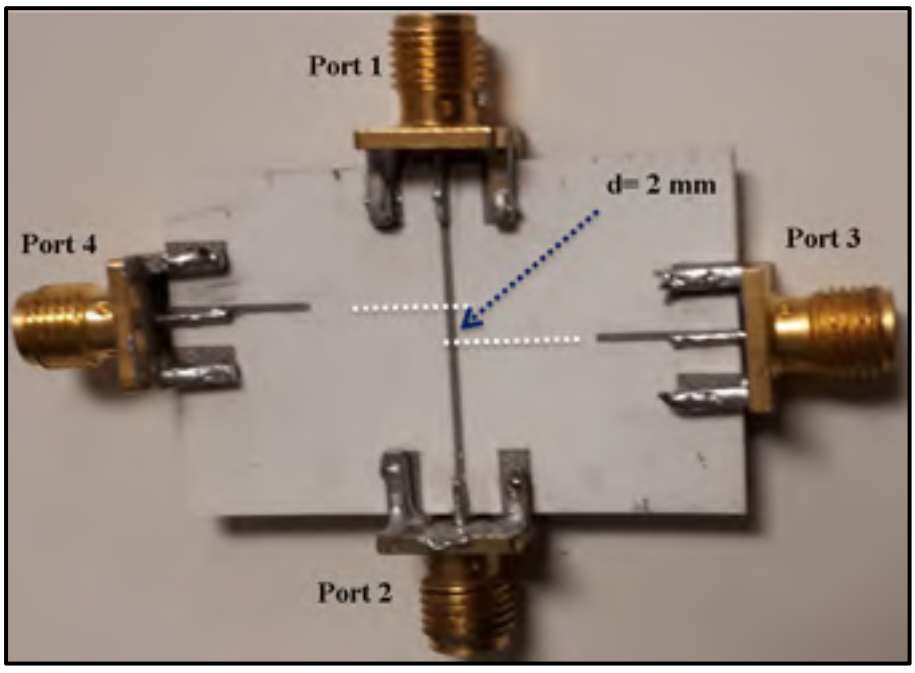

Figure 3.29Photograph of proposed 4-port reflectometer

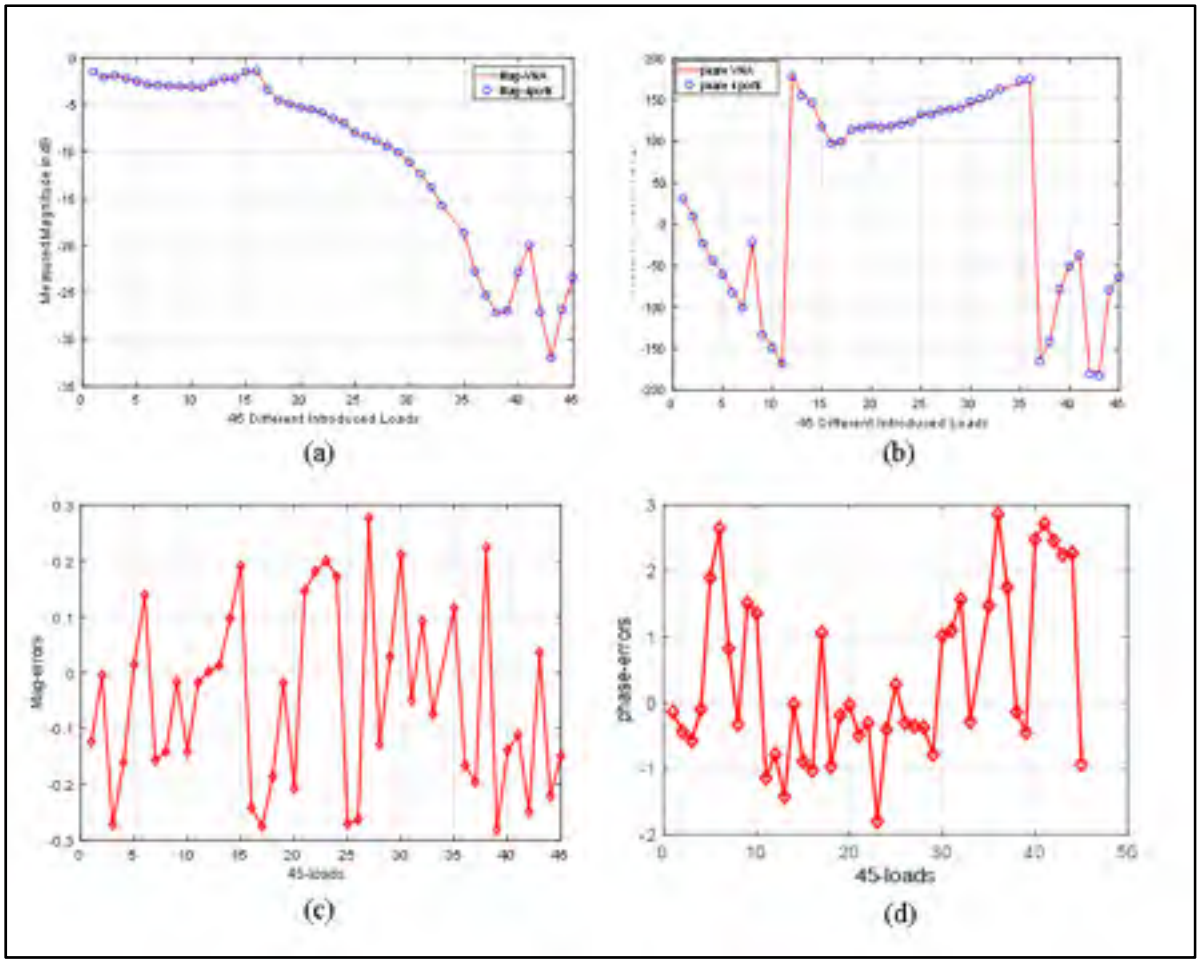

Figure 3.30(a) measured magnitude and (b) phase of reflection coefficient of different 45 loads, and its errors in magnitude (c) and phase (d) for version 2 reflection coefficient measurement with errors around 0.3 dB in magnitude and 3^0 in phase

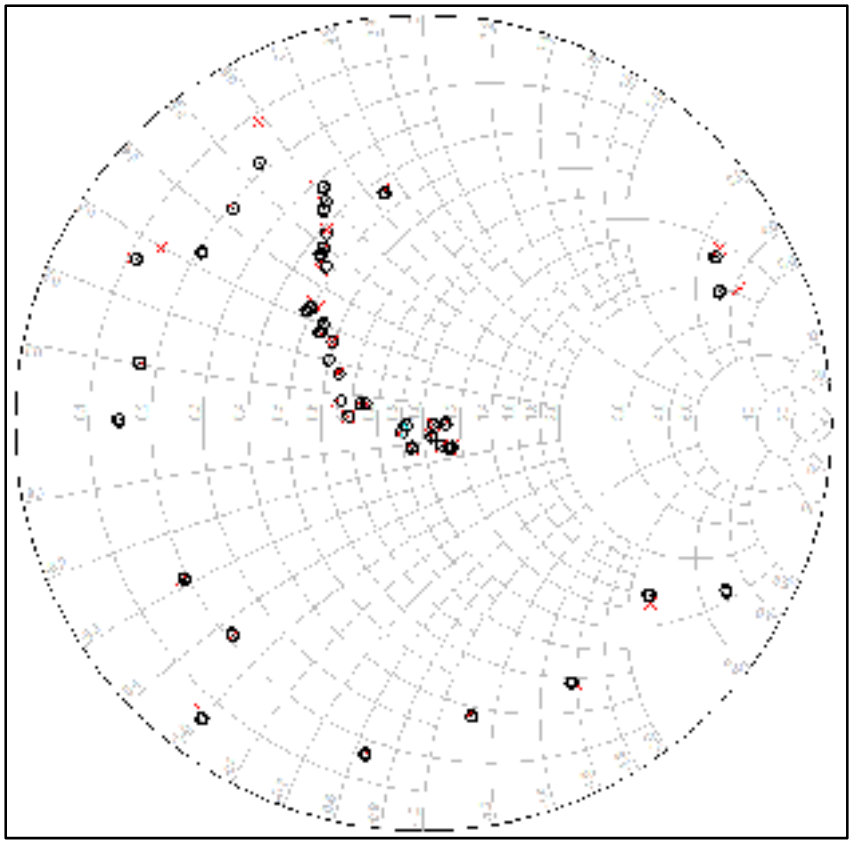

Figure 3.31 Measurement results of the reflection coefficient plotted on smith chart

CONCLUSION

Microwave engineering is improved to work in several most recent wireless systems with wide focus on better use of electromagnetic spectrum in different research interest. Vector network analyzer is reviewed as a traditional technique for vector measurement. Another alternative technique for vector measurement is found in six-port technique and gain and phase detection circuits are presented as well as the four-port interferometer as an alternative solution for embedded vector measurement that is characterized with very small size, very low coupling, and integrated for embedded measurement with a good agreement results in amplitude and phase is presented.There are different techniques or solutions for providing RF vector measurement such as six-port junction, vector network analyzer, and phase and gain detection which are reviewed. Despite the high accuracyand wideband measurement over the frequency range of these techniques, they use directional coupler and other microwave components which make the device bulky in size with high losses. Thus, the alternate solution which is established based on non-directional 4-port reflectometer using sniffers which is characterized with very small size and non-directional which can be sited at minimum destination in order to measure the reflection coefficient is reviewed. A new 3D optimized 4-port non-directional reflectometer for measuring complex reflection coefficients is proposed. The proposed reflectometer features two optimized non-directional sniffers positioned in 3D below a transmission line with buried lines to carry the sniffed signals to power detectors in LTCC technology. Vertical transitions from the buried lines to surface Microstriplines are designed and optimized. 3D electromagnetic field simulations HFSS are used to optimize the proposed design to get the S-parameters of the structure. Two LT5582 with 57 dBm dynamic range are used to detect the coupled power where the S-parameters and measured power are used as a part of the algorithm to compute the reflection coefficient of the DUT. A prototype of the proposed reflectometer is fabricated in LTCC in LACIME laboratory and utilized to measure 45 different complex loads. The obtained results present an excellent agreement with VNA measurements showing errors below 0.3 dB for amplitude and below 3° for phase.The non-directional four-port reflectometer is highly recommended for circuit integration because of its characteristics from small size and less losses. The accuracy of the measurement was accepted for ideal RF embedded system

Future Work

- Instead of having the proposed 3D reflectometer and the LT5582 power detector circuit connecting together by SMA 50 Ohm connectors during the measurement process, it will be new approach when both circuits are integrated in one chip/circuitrydesign using multilayer substrate of LTCC technology where the resistors and capacitors components (RC) will be embedded within the LTCC substrate.
- Performingfull two-port measurement system where the two circuits of the proposed 3D reflectometer will place at the input and the output of the DUT.

APPENDIX I

3D Reflectometer Design for Embedded RF Vector Measurement

Hana S. Mohamed, Ammar B. Kouki

Communication and Microelectronics Laboratory (LACIME)

Electrical Engineering Department

École de Technologie Supérieure

Montréal, Québec, Canada

hana.mohamed.1@ens.etsmtl.ca

***Abstract* — a novel 3D 4-port non-directional reflectometer for measuring complex reflection coefficients is proposed. The proposed reflectometer features two optimized non-directional sniffers positioned below a transmission line with buried lines to carry the sniffed signals to power detectors in LTCC technology. Vertical transitions from the buried lines to surface microstrip lines are designed and optimized. 3D electromagnetic field simulations are used to optimize the proposed design. A prototype of the proposed reflectometer is fabricated and used to measure 45 different complex loads. The obtained results show excellent agreement with VNA measurements showing errors below 0.3 dB for amplitude and below 3° for phase.**

***Index Terms* — Reflectometer, Reflection coefficient, coupled power, LTCC.**

I INTRODUCTION

Microwave engineering and applications have continued to grow over the last few years fueled by growth in many wireless systems such as 5G and the Internet of Things (IoT). Along with this growth, the need for embedded measurements of RF circuits and devices has also been increasing. In particular, embedded vector RF measurements, traditionally only accessible with commercial vector network analyzers [1], are needed to enable in situ monitoring and reconfiguring RF circuits and systems. Another classic approach is the 6-port method [2], which uses several individual power measurements to perform vector measurements of reflection coefficients. While either of the above-mentioned methods can be used with relative success, they have their drawbacks. As discussed, vector network analyzers are expensive, but they are also somewhat difficult to purchase commercially, while the 6-port method requires two directional couplers and multiple power dividers, which can lead to a large size not suitable for embedding in RF front-end circuitry. In 2010, a new approach was investigated in which a four-port reflectometer using non-directional signal sniffers were used leading to small size that is more convenient for embedded circuit integration [3]. This reflectometer was based on a planar circuit design where the sniffers were placed close to the signal-carrying

Microstripline. This configuration provided relatively good performance with magnitude error less than 0.8 dB and phase error less than 6º. However, the presence of the sniffing lines in the same layer as the signal-carrying lines maybe inconvenient when additional signal or bias lines need to be routed on the same layer. In this work, a new four-port reflectometer structure that uses 3D sniffers in LTCC technology, which do not interfere with the signal/bias carrying lines, is proposed. 3D electromagnetic field simulation is used to optimize the proposed sniffers and their vertical transitions to the surface. Validation of the designs with LTCC fabricated 3D.

II PROPOSED 3D 4-PORT REFLECTOMETER

The proposed system is shown in Fig. 1 and comprises a 3D 4-port reflectometer made up of a transmission line (TL) connected to the source (port 1), the device-under-test (DUT) (port 2) and two non-directional sniffers (ports 3 and 4) made of partially filled vais positioned underneath the TL and separated by a distance d, which should be much less than λ/4. This configuration insures that there is no interference between the surface components and the sniffers. Two RMS power detector circuits (LT5582 [4]) are placed at ports 3 and 4 to measure the sampled powers.

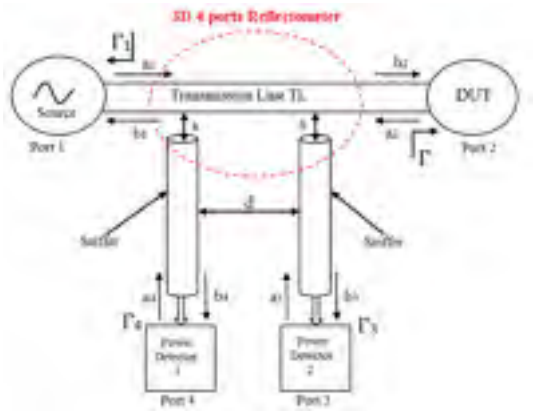

Fig. 1.3D four-port reflectometer configuration.

A Reflection Coefficient Determination

First, for a given reflectometer geometry as shown in Fig. 1, its S-parameters can be obtained through 3D field simulation or measurements. These S-parameters are then combined with the measured powers at ports 3 and 4 of the passive sniffers to compute the complex reflection coefficient of the DUT at port 2.

$$\Gamma_L = \frac{a_2}{b_2} = x + jy \qquad (1)$$

The measured powers at ports 3 and 4 are related to the waves b_3 and b_4 by:

$$\begin{cases} P_3 = |b_3|^2 \\ P_4 = |b_4|^2 \end{cases} \qquad (2)$$

To compute Γ_L, first the transmission coefficients between port 1 and ports 3 and 4, $T_{31}$and T_{41}, respectively, are expressed as follows using a signal flow graph and Mason's rule [3]-[5]:

$$T_{31} = \frac{b_3}{a_1} = \frac{A_1\Gamma_L + B_1}{C\Gamma_L + D} \qquad (3)$$

$$T_{41} = \frac{b_4}{a_1} = \frac{A_2\Gamma_L + B_2}{C\Gamma_L + D} \qquad (4)$$

Based on these equations, and assuming good matching at all ports, the six parameters of A_1, A_2, B_1, B_2, C and D can be determined from:

$$\begin{bmatrix} A_1 & A_2 \\ B_1 & B_2 \\ C & D \end{bmatrix} = \begin{bmatrix} (S_{21}S_{32} - S_{31}S_{22}) & (S_{21}S_{42} - S_{41}S_{22}) \\ S_{31} & S_{41} \\ -S_{22} & 1 \end{bmatrix} \qquad (5)$$

Thus, by inserting (3) and (4) into (2), the measured powers at ports 3 and 4 can be written as:

$$\begin{cases} P_3 = P_1 \left| \frac{A_1\Gamma_L + B_1}{C\Gamma_L + D} \right|^2 \\ P_4 = P_1 \left| \frac{A_2\Gamma_L + B_2}{C\Gamma_L + D} \right|^2 \end{cases} \qquad (6)$$

Next, to calculate Γ_L, we explicit equations (6) in terms of the its real and imaginary parts as follows:

$$(x - \alpha_3)^2 + (y - \beta_3)^2 = r_3^2 \qquad (7)$$

$$(x - \alpha_4)^2 + (y - \beta_4)^2 = r_4^2 \qquad (8)$$

Where α_3, β_3, α_4, β_4, r_3, and r_4 six actual parameters that can be presented in the expression of A_1, B_1, A_2, B_2, C, D, and P_1, and Q_3 and Q_4 are the center of the circles.

Equations (7, 8) are equations of circles in the complex Γ plane as shown in Fig. 2. To ensure that these equations have a solution, both circles must intersect. This requires that the spacing between the sniffers, d, be in an appropriate range as shown in [3]. Once this condition is stratified, there will be two intersections with one being inside the unit circle while the second is outside of it. For passive loads the following condition must also be satisfied:

$$\left|\Gamma_L\right|^2 = x^2 + y^2 \le 1 \qquad (9)$$

Hence, the DUT's Γ_L can be determined by selecting the intersection point inside the unit circle.

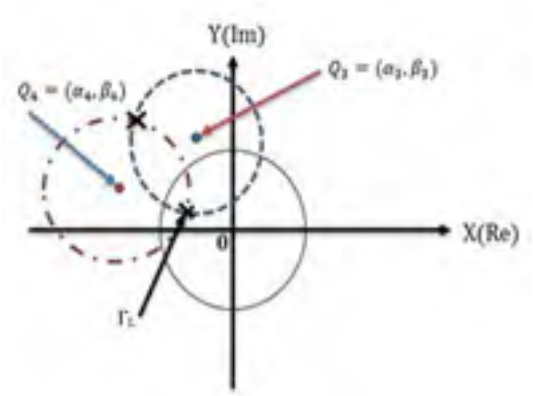

Fig. 2. Intersection for the two circles in Γ plane to calculate reflection coefficient.

B Transition Design

Fig. 3 shows the 3D model of the proposed reflectometer designed to operate between 1 and 3 GHz in LTCC technology. Four layers of Ferro L8 (ε_r = 7.2) are used in this desing. The sniffers are filled vias in layers 2 and 3. The microstripline is on top the fourth layer while buried line to ports 3 and 4 are on layer 1. As can be seen, the sniffers are made of partially filled vias that are under the microstripline but do not touch it. One important design consideration is the matching of the transtions at ports 3 and 4, shown in a close-up view in Fig. 3 as well. 3D field simulation was used to optimize this transition, which is a type of microstrip-to-strpiline transition [6]. Fig. 4 shows the 3D model of the optimized desing of two back-to-back transitions suitable for fabrication measurement. Fig. 5 shows two fabricated models of this design while Fig. 6 presents the measurement results with good matching for the desired band. Slight dissemtry is observed due to the LTCC fabircation process.

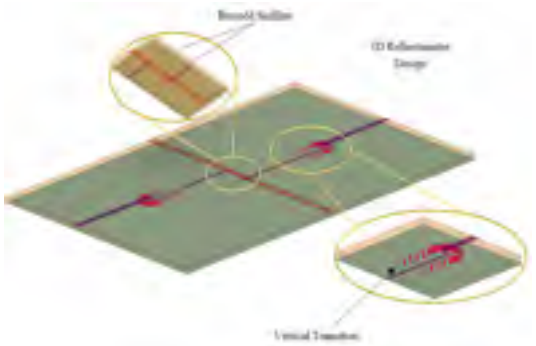

Fig. 3. 3D model of the full reflectometer with buried sniffers and vertical transition.

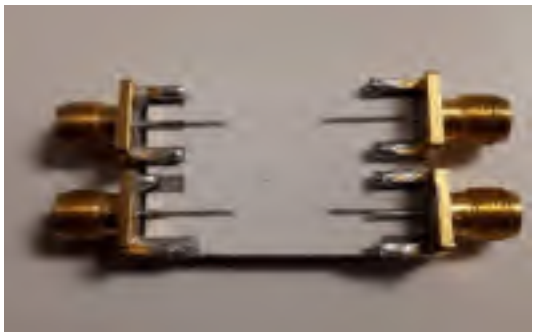

Fig. 4.Photo of prototype of Microstripline-to-buried line-to- Microstripline.

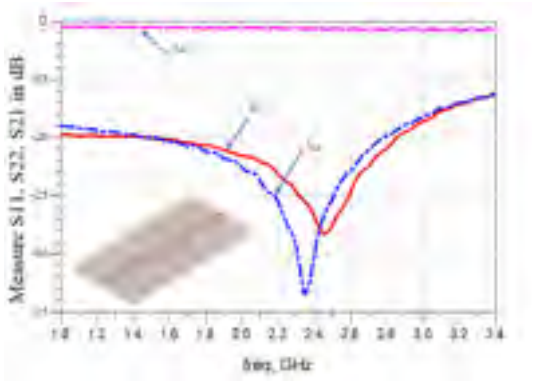

Fig. 5.Measured S-parameters for prototype of microstripline-to-buried line-to-microstripline.

C Reflectometer Design and Fabrication

Once the transitions have been optimized, the full reflectometer structure, shown in Fig. 3, is designed and optimized. This consists of (i) optimizing the layer thicknesses to ensure that the sniffers achieve a coupling level on the order 30 dB and (ii) proper dimensioning of the

spacing between the sniffers to ensure small size and good operation in the desired frequency band. The optimization of the sniffer to microstrip line spacing was achieved with a vertical separation of 89 μm, corresponding to a single 5-mil layer (before sintering). For sniffer spacing, a distance of 2 mm (or λ/40) was found to provide good operation with small size. Fig. 6 shows the fabricated reflectometer with the through microstrip line and the buried sniffers and optimized transitions.

MEASUREMENT RESULTS

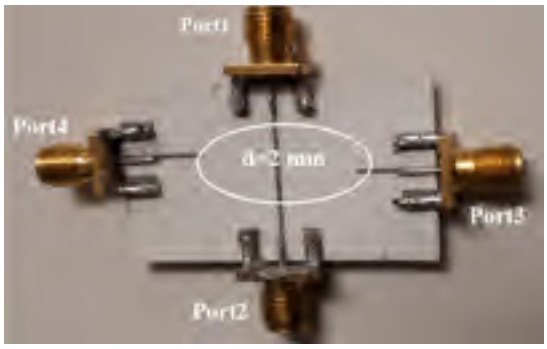

Fig. 6. Fabricated 3D reflectometer.

To validate the operation of the fabricated 3D reflectometer, it's measured four-port S-parameters are first measured and stored. Next, a double stub tuner terminated by 50 Ω at one its ports is used to present a one port load of varying impedance. For a given tuner setting, a commercial vector network analyzer (Agilent VNA HP8753ES) is used to measure the corresponding load impedance. At the same setting, the tuner is then placed at port 2 of the reflectometer while port one is excited with signal generator (Agilent HPE4438C). The powers at ports 3 and 4 are measured using two LT5582 power detectors with a dynamic range of 57 dB. The measured powers and reflectometer S-parameters are then used as described in Section II.A to determine the load impedance. In total, 45 different loads were measured at 1.2 GHz. Fig. 7 shows a comparison between the VNA- and reflectometer-measure magnitudes of the reflection coefficient. Excellent agreement is observed with the difference not exceeding 0.3 dB for all 45 measured loads. Similarly, very good agreement is observed in the measured phase of the reflection coefficient between the VNA and the reflectometer for all measured loads with the difference between the two not exceeding 3° as shown in Fig. 8.

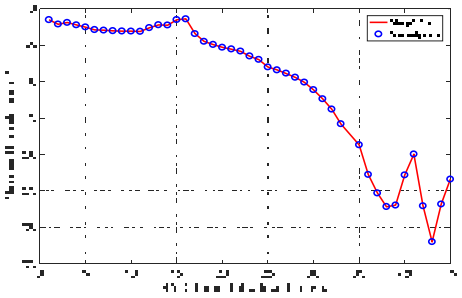
Fig. 7.Measured magnitude of Γ in dB.

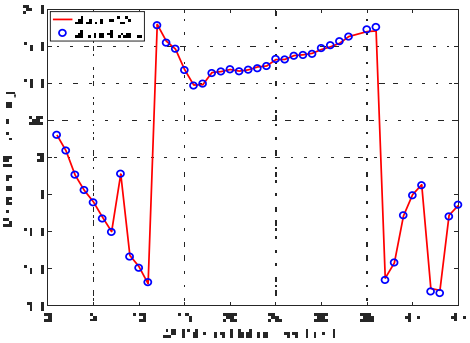
Fig. 8.Measured phase of Γ in degrees.

CONCLUSION

A novel four-port reflectometer realizable in 3D LTCC technology was proposed. The design of the reflectometer and the optimization of the 3D transitions needed for its operation were carried out using 3D electromagnetic field simulation. The optimization of the transitions was validated through fabrication and measurement of two back-to-back transitions. The operation and precision of the proposed reflectometer were demonstrated by comparing the measured reflection coefficient of 45 different complex loads with the proposed reflectometer and a commercial VNA. Given the its small size, the nature of its buried sniffers and the precision of the results it provided, the proposed reflectometer is well-suited of

integration into RF front-end circuits to provide embedded measurements.

*A*CKNOWLEDGEMENT

The authors wish to acknowledge the generous support of Ferro in research conducted at the LACIME labs.

*R*EFERENCES

[1] *D. Fei, "Research of influence of several factors on dynamic range of vector network analyzer," 2013 IEEE 11th International Conference on Electronic Measurement & Instruments, Harbin, 2013, pp. 366-369.*

[2] *F. M. Ghannouchi and A. Moahmmadi, The Six-Port Technique With Microwave and Wireless Applications, MA: Artech House, 2009*

[3] *A. B. Kouki, I. Masri, F. Gagnon and C. Thibeault, "On the embedded vector RF measurements in frequency agile and reconfigurable front-ends," 5th International Conference on Design & Technology of Integrated Systems in Nanoscale E, 2010,pp. 1-5.*

[4] *Analog Devices "40MHz to 10GHz RMS Power Detector with 57dB Dynamic Range LT5582"ANALOG DEVICES, INC. 2010-2018 D17029-0-6/18(A) www.analog.com.*

[5] *G. Gonzalez, "Microwave transistor amplifier," Prentice-hall., second edition, pp. 175-185, 1997. G. F. Engen, "The six-port reflectometer: An alternative network analyzer," IEEE Trans. Microwave Theory & Tech., vol. MTT-25, no. 12, pp. 1075-1080, December 1977.*

[6] *Huang, S. Zhang and W. Jiang, "A shielded microstrip-to-stripline vertical transition for multilayer printed circuit board," 2012 International Conference on Microwave and Millimeter Wave Technology (ICMMT), Shenzhen, 2012, pp. 1-3.*

APPENDIX II

MATLAB CODES TO COMPUTE THE REFLECTION COEFFICIENT OF THE DEVICE UNDER TEST

```
ZL=100+60i;
gamma=(ZL-50)/(ZL+50);
%***************** part 1 for 1.2 GHz **************
%******** step 1: insert the S parameters ******
S21dB=-0.12; S21Phase=175.2722°;
S22dB=-30.385 ; S22Phase=39.037°;
S31dB=-29.757; S31Phase=-174.480°;
S32dB=-29.781; S32Phase=-43.980°;
S41dB=-30.363; S41Phase=-167.271°;
S42dB=-30.450; S42Phase=-54.176°;
S21M=10^(S21dB/20);
S22M=10^(S22dB/20);
S31M=10^(S31dB/20);
S32M=10^(S32dB/20);
S41M=10^(S41dB/20);
S42M=10^(S42dB/20);
% S11M=10^(S11dB/20);
% ******convert from dB to linear*****
S21 = (S21M)*exp(1i*S21Phase*pi/180);
S32 = (S32M)*exp(1i*S32Phase*pi/180);
```

```
S31 = (S31M)*exp(1i*S31Phase*pi/180);
S22 = (S22M)*exp(1i*S22Phase*pi/180);
% S11 = (S11M)*exp(1i*S11Phase*pi/180);
S41 = (S41M)*exp(1i*S41Phase*pi/180);
S42 = (S42M)*exp(1i*S42Phase*pi/180);
%******** step 2: parameters calculation ******
A1 = S21*S32 - S31*S22 ;
A2 = S21*S42-S41*S22 ;
B1= S31 ;
B2= S41 ;
C= -S22 ;
D= 1 ;
Real and imaginary part
A2r=real(A2); A2i=imag(A2);
A1r=real(A1); A1i=imag(A1);
B2r=real(B2); B2i=imag(B2);
B1r=real(B1); B1i=imag(B1);
Cr=real(C); Ci=imag(C);
Dr=real(D); Di=imag(D);

%*****input power and power at P3andP4*****

P3dBm = -26.547;
P1dBm =0;
```

```
P4dBm = -27.521;

%**************convert power from dBm to mW

P1 = 10^(P1dBm/10)/1000;P3 = 10^(P3dBm/10)/1000;

P4 = 10^(P4dBm/10)/1000;

Power at port 3 and 4

Pr31=P3/P1;

Pr41=P4/P1;
```

Circle equations to find Γ_L

```
alpha3=-((Dr*Cr+Di*Ci)*Pr31-(B1r*A1r+B1i*A1i))/(Pr31*(Cr^2+Ci^2)-(A1r^2+A1i^2));

beta3=-((Di*Cr-Dr*Ci)*Pr31-(B1i*A1r-B1r*A1i))/(Pr31*(Cr^2+Ci^2)-(A1r^2+A1i^2));

R3= sqrt((((B1i^2+B1r^2)-(Dr^2+Di^2)*Pr31)/(Pr31*(Cr^2+Ci^2)-
(A1r^2+A1i^2)))+alpha3^2+beta3^2);


alpha4=-((Dr*Cr+Di*Ci)*Pr41-(B2r*A2r+B2i*A2i))/(Pr41*(Cr^2+Ci^2)-(A2r^2+A2i^2));

beta4=-((Di*Cr-Dr*Ci)*Pr41-(B2i*A2r-B2r*A2i))/(Pr41*(Cr^2+Ci^2)-(A2r^2+A2i^2));

R4=sqrt((((B2i^2+B2r^2)-(Dr^2+Di^2)*Pr41)/(Pr41*(Cr^2+Ci^2)-
(A2r^2+A2i^2)))+alpha4^2+beta4^2);
```

%.....Plotting Circles of Γ_L….

```
h1 = plotcircle(alpha3,beta3,R3,'r');
```

```
holdon
h2 = plotcircle(alpha4,beta4,R4,'b');
holdon
plotcircle(0,0,1,'-g');
holdon
plotcircle(real(gamma),imag(gamma), 0.05, '-b');
gridon
```

LIST OF BIBLIOGRAPHICAL REFERENCES

F. Domingue, S. Fouladi, A. B. Kouki and R. Mansour, 2009 “Design Methodology andOptimizationof DMTL Impedance Matching Networks for Low Frequency Applications,” IEEE Trans. OnMicrowave Theory and Techn, vol. 57, no. 12, pp.

N. Chagtmi, N. Boulejfen and F. M. Ghannouchi, 2017 "Conception of a Dual-band Six-portBasedReflectometer," 2017 Mediterranean Microwave Symposium (MMS), Marseille, 2017, pp. 1-4.doi: 10.1109/MMS.2017.8497162.

V. Kible, K. B. de Brito and R. N. de Lima, 2017"Quadrature frontend with directional coupler for RF reflection coefficient measurements," 2017 SBMO/IEEE MTT-SInternational Microwave andOptoelectronics Conference (IMOC),AguasdeLindoia, pp. 1-5.doi: 10.1109/IMOC.2017.8121102.

M. Randus and K. Hoffmann, 2007"A simple method for extremeimpedances measurement," 2007 70th ARFTG Microwave Measurement Conference(ARFTG), Tempe, AZ, 2007, pp. 1-5.czxc doi:10.1109/ARFTG.2007.8376178.

R. Malmqvist et al., 2010 "RF MEMS and MMIC based reconfigurable matching networks for adaptive multi-band RF front-ends," 2010IEEE International Microwave Workshop Series on RF Front-ends forSoftware Defined and Cognitive Radio Solutions (IMWS), Aveiro, pp. 1-4.

A. Eroglu, R. Goulding, P. Ryan, J. Caughman and D. Rasmussen,2010 "Novel broadband multilayer microstrip directional couplers," 2010 IEEE Antennas and Propagation Society International Symposium, Toronto, ON, pp. 1-4.

A. B. Kouki; I. Masri ; F. Gagnon; C. Thibeault, 2010“On the Embedded Vector RF Measurements in Frequency Agile and Reconfigurable Front-Ends”, 5th International Conference on Design & Technology of Integrated Systems in Nanoscale Era, Hammamet, Tunisia, pp. 1-5.

H. Okazaki, A. Fukuda, K. Kawai, T. Furutaamd S. Narahashi, 2007 “Reconfigurable RF Circuits for Future Band-Free Mobile Terminals,” IEEE Int. Symp. On Signals, systems and Electronics, Montreal, Canada, pp. 99-102.

Z. Feng et. al, 2009 “Narrowband Barium Strontium Titanate (BST) Tunable Bandpass Filters a X-band,” IEEE Int. Microwave Symposium, Boston, USA, pp. 10611064.

F. M. Ghannouchi and A. Moahmmadi, 2009 “The Six-Port Technique With Microwave an Wireless Applications, MA: Artech House.

T. Hentschel, 2005 “The Six-Port as a Communications Receiver, 2005” IEEE Trans. On Mirowave Theory and Techniques, vol. 53, no. 3, pp. 10391047.

Y. Cassivi, F. M. Ghannouchi, and R. G. Bosisio,, 1992 “Six-Port Junctions in a Phased Array Antenna for Accurate Beamsteering,” IEEE. Antennas & Propagation International Symposium, Chicago, USA, pp. 462-465.

Analog Devices, “LF-2.7 GHz RF/IF Gain and Phase Detector AD8302”, 2002.

M. Arshad .and A. Kouki, 2006 “Precise estimation of MIMO channel capacity from RF measurements,” Wireless Technology, 2006. The 9th European Conference, pp. 209

J. Rodriguez-Tellez, 1992 “Microwave probe for circuit/device testing,” Circuits, Devices and Systems, IEE Proceedings G, vol. 139, no. 3, pp. 333-338.

G. Gonzalez, “Microwave transistor amplifier, 1997” Prentice-hall., second edition, pp. 175 185.

G. F. Engen, 1977 “The six-port reflectometer: An alternative network analyzer,” *1*977 IEEE MTT-S International Microwave Symposium Digest, San Diego, CA, USA, 1977, pp. 44-46. doi: 10.1109/MWSYM.1977.1124352G.

F. Engen, 1976 “Determination of Microwave Phase and Amplitude From Power Measurement”,in IEEE Transactions on Instrumentation and Measurement, vol. IM-25, no4, pp. 414-418, Dec. 1976. doi: 10.1109/TIM.1976.6312254.

K. Staszek, S. Gruszczynski, K. Wincza, 2013 “Theoretical Limits and Accuracy Improvement of Reflection-Coefficient Measurements in Six-Port Reflectometers”, IEEE Transactions on Microwave Theory and Techniques, vol. 61, no.

S. O. Tatu, K. Wu, 2013“Six Port Technology and Applications”,Telsiks F. M. Ghannouchi, A. Mohammadi, 2009 “The Six Port Technique”,Artech House.

L. Samuel, 1947 “An oscilloscope method of presenting impedances on the reflectioncoefficient plane,” Proc. IRE, vol. 35, pp.

S. B. Cohn and N. P. Weinhouse, 1964 “An automatic microwave phase measurement system,” Microwave Journal,vol. 7, pp. 49–56.

C. A. Hoer, 1972 “The 6-port coupler: A new approach to measuring voltage, current, power, impedance, and phase,” IEEE Transactions on Instrumentation and Measurements, vol. IM-21.

G. F. Engen and C. A. Hoer, 1972 “Application of an arbitrary six-port junction to power measurement problems,” IEEE Transactions on Instrumentation and Measurements ,vol. IM21.

C. A. Hoer, 1977 “A Network Analyzer Incorporating Two Six Port Reflectometers”,IEEETransactions on Microwave Theory and Techniques, vol. MTT-25, no.12, pp. 1070-1074, Dec. 1977.doi: 10.1109/TMTT.1977.1129276.

G. F. Engen, 1977 "The Six-Port Reflectometer: An Alternative Network Analyzer," in *IEEE* Transactions on Microwave Theory and Techniques, vol. 25, no. 12, pp. 1075-1080, doi: 10.1109/TMTT.1977.1129277.

G. F. Engen,1977 “An Improved Circuit for Implementing the Six-Port Technique of Microwave Measurements”, IEEE Transactions on Microwave Theory and Techniques, vol. MTT-25, no.12, pp. 1080-1083,doi: 10.1109/TMTT.1977.1129278.

E. R. B. Hansson, G. P. Riblet, 1983 “An Ideal Six-Port Network Consisting of a Matched Reciprocal Lossless Five-Port and a Perfect Directional Coupler”, IEEE Transactionson Microwave Theory and Techniques, vol. MTT-31, no.3, pp. 284-288. doi: 10.1109/TMTT.1983.1131477.

A. Koelpin, G. Vinci, B. Laemmle, D. Kissinger, and R. Weigel, 2010 “The six-port in modern society”, IEEE Microwave Magazine, vol. 11, no. 7, pp. 35-43, Dec. 2010. doi: 10.1109/MMM.2010.938584.

P. J. Probert, J. E. Carroll, 1982 “Design features of multi-port reflectometers”, Microwaves, Optics and Antennas, IEE Proceedings*H - Microwaves, Optics and Antennas*, vol. 129, no. 5, pp. 245-252, October 1982. doi: 10.1049/ip-h-1:19820050.

G. F. Engen, 1977"The Six-Port Reflectometer: An Alternative Network Analyzer," 1977 IEEE MTT-S International Microwave Symposium Digest, San Diego, CA, USA, pp. 44-46.doi: 10.1109/MWSYM.1977.1124352.

W. W. Mumford, 1947"Directional Couplers," in Proceedings of the IRE, vol. 35, no. 2, pp. 160-165. doi: 10.1109/JRPROC.1947.231592.

B. A. Galwas, 1975“Measurement of Reflection Coefficient by Means of Line and HomodynDetection System”, IEEE Transactions on Instrumentation and Measurement, vol.IM-24, no. 3.

R. J. King, R. I. Christopherson, 1970 “Homodyne System for the Measurement of Microwave Reflection Coefficients”, in IEEE Transactions on Microwave Theoryand Techniques, vol. 18, no. 9, pp. 658-660, September 1970. doi: 10.1109/TMTT.1970.1127311.

G. H. Glover, 1970 “Simple Technique for Real-Time Measurement of Complex Reflection Coefficient”, in IEEE Transactions on Microwave Theory and Techniques, vol. 18, no. 7, pp. 410-412, July 1970. doi: 10.1109/TMTT.1970.1127254.

K. Hoffmann, 1998“A Novel Vector Network Analyzer”, IEEE Transactions on Microwave Theory and Techniques, vol. 46, no. 12.

L. C. Oldfield, 1985 “A Multistate Reflectometer”, in IEEE Transactions on Instrumentation and Measurement, vol. IM-34, no. 2, pp. 198-201. doi: 10.1109/TIM.1985.4315301

S. Li, R. G. Bosisio,1983 “The Measurement of Complex Reflection Coefficient by Means of a Five-Port Reflectometer”, IEEE Transactions on Microwave Theory and Techniques, vol. MTT-31, no. 4.

E. Martin, J. Margineda, J. M. Zamarro, 1982“An Automatic Network Analyzer Using a Slotted Line Reflectometer”, IEEE Transactions on Microwave Theory and Techniques, vol. MTT-30, no. 5.

Y. Cassivi, F. M. Ghannouchi, and R. G. Bosisio, 1992 “Six-Port Junctions in a Phase Array Antenna for Accurate Beamsteering,” IEEE. Antennas & Propagation International Symposium, Chicago, USA, pp. 462-465 vol.1.doi: 10.1109/APS.1992.221900

C. Gutierrez Miguelez, B. Huyart, E. Bergeault and L. P. Jallet, 2000 "A new automobile radar based on the six-port phase/frequency discriminator, " in IEEE Transactionson Vehicular Technology, vol. 49, no. 4, pp. 1416-1423, doi: 10.1109/25.875273.

Analog Devices 2002"LF–2.7 GHz RF/IF Gain and Phase Detector AD8302" One Technology Way, P.O. Box 9106, Norwood, MA 02062-9106, U.S.A.www.analog.com © Analog Devices, Inc.

N. Instruments,2014 "Introduction to Network Analyzer Measurements," in Fundamentals and Background.

Tektronix, 2017 "Network Analyzer Measurements Fundamentals".

D. Fei, 2013"Research of influence of several factors on dynamic range of vector network analyzer," 2013 IEEE 11th International Conference on Electronic Measurement & Instruments, Harbin, pp. 366-369.

R. Zitouni and L. George,2016 "Output power analysis of a software defined radio device,″ 2016 IEEE Radio and Antenna Days of the Indian Ocean (RADIO), St. Gilles-les-Bains, pp. 1-2. doi: 10.1109/RADIO.2016.7771996.

C. Park, S. Kim, S. Lim and M. Song, 2007 "HMM Based Channel Status Predictor for Cognitive Radio," 2007 Asia-Pacific Microwave Conference, Bangkok, pp. 1-4. doi: 10.1109/APMC.2007.4554696.

Wee Chang Khor and M. E. Bialkowski, 2006 "Investigations into cylindrical and planar configurations of a microwave imaging system for breast cancer detection," 2006 IEEE Antennas and Propagation Society International Symposium, Albuquerque, NM, pp. 263-266.doi: 10.1109/APS.2006.1710506.

W. C. Khor, M. E. Biakowski, A. Abbosh, N. Seman and S. Crozier, 2007 “An Ultra wideband microwave imaging system for breast cancer detection”, IEICE Trans. Commun. Vol. E85-A/B/C/D, no. 1.

B. Sopori, Yi Zhang, Wei Chen and J. Madjdpour, 2000 "Silicon solar cell process monitoring by PV-reflectometer," Conference Record of the Twenty-Eighth IEEE Photovoltaic Specialists Conference - 2000 (Cat. No.00CH37036), Anchorage, AK, USA, pp.120-123.doi: 10.1109/PVSC.2000.915769.

G. Vinci and A. Koelpin, 2016 "Progress of Six-Port technology for industrial radar applications," 2016 IEEE Topical Conference on Wireless Sensors and Sensor Networks(WiSNet),Austin,TX, pp.48-51. doi:10.1109/WISNET.2016.7444319.

N. A. Zulkifli, N. Khalid, S. Z. Ibrahim and G. S. Tan,2016 "Development of six-port baseband processing system for short range radar based sensor," 2016 3rd International Conference on Electronic Design (ICED), Phuket, pp.400-403.doi: 10.1109/ICED.2016.7804677.

C. Nieh, T. Huang and J. Lin,2014 "Antenna radiation pattern effects on a short-range vibration-detection radar system," 2014 International Symposium on Antennas and Propagation Conference Proceedings, Kaohsiung, pp.135-136.doi: 10.1109/ISANP.2014.7026567.

K. Hoffmann and Z. Skvor, 1998"A novel vector network analyzer, 1998" IEEE MTT-S International Microwave Symposium Digest (Cat. No.98CH36192), Baltimore, MD, USA, 1998, pp. 953-956 vol.2.doi: 10.1109/MWSYM.1998.705149.

W. S. Abdulrab, M. R. Islam, M. H. Habaebi and M. M. Ahmed, 2016"Design of Multiple Input Multiple Output Patch Antenna for Multiband Applications," 2016 International Conference on Computer and Communication Engineering (ICCCE), Kuala Lumpur, pp. 13-18.doi: 10.1109/ICCCE.2016.17.

H. Okazaki, T. Furuta, K. Kawai, Y. Takagi, A. Fukuda and S. Narahashi, 2013 "Reconfigurable RF circuits for future multi-mode multi-band mobile terminals," 2013 International Symposium on Electromagnetic Theory, Hiroshima, pp. 432-435.

F. Domingue, S. Fouladi, A. B. Kouki and R. Mansour, 2009 “Design Methodology and Optimization of DMTL Impedance Matching Networks for Low Frequency Applications,” IEEE Trans. on Microwave Theory and Techn., vol. 57, no. 12, pp. 3030-3041.